THE UNIVERSITY OF ST. ANDREWS

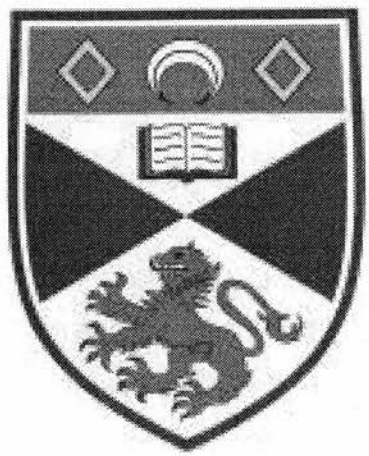

Stellar Magnetic Fields

Thomas McIvor

Submitted for the degree of Ph.D.

September 20, 2005

DECLARATION

I, Thomas McIvor, hereby certify that this thesis, which is approximately 20000 words in length, has been written by me, that it is the record of work carried out by me and that it has not been submitted in any previous application for a higher degree.

September 20, 2005

I was admitted as a research student in October 2001 and as a candidate for the degree of Ph.D. in October 2001; the higher study for which this is a record was carried out at the University of St. Andrews between 2001 and 2005.

September 20, 2005

In submitting this thesis to the University of St. Andrews I understand that I am giving permission for it to be made available for use in accordance with the regulations of the University Library for the time being in force, subject to any copyright vested in the work not being affected thereby. I also understand that the title and abstract will be published, and that a copy of the work may be made and supplied to any *bona fide* library or research worker.

September 20, 2005

I hereby certify that the candidate has fulfilled the conditions of the Resolution and Regulations appropriate for the degree of Ph.D. in the University of St. Andrews and that the candidate is qualified to submit this thesis in application for that degree.

September 20, 2005

ACKNOWLEDGMENTS

It is with pleasure that i would like to thank my supervisor, Dr. Moira Jardine. Over these past 4 years her encouragement, guidance and patience and been invaluable. I would also like to thank Dr. Volkmar Holzwarth who in the last 2 years has provided much insight and inspiration. This brings me to my family, in particular i would like to thank my Dad who's constant support and belief in me has been a real driving force to finish this PhD. Thankyou to my wife Cam, who on days when my idleness grew strong, was ultimately responsible for making me get up in the morning and go to university. Thankyou to my Mum and Margaret and all my brothers and sisters for their love and support. Finally, i would like to gratefully acknowledge the financial support of PPARC.

THE UNIVERSITY OF ST. ANDREWS

Stellar Magnetic Fields

Submitted for the degree of Ph.D.

September 20, 2005

Thomas McIvor

ABSTRACT

This thesis is dedicated to the theoretical study of stellar magnetic fields. In particular we look at the affect the coronal magnetic field of a star can have on observable parameters. These include features such as Prominences, X-ray emission, cyclic behavior and planet-star magnetic interactions. By studying the structure and effects of the magnetic field we gain a deeper understanding of stellar evolution.

To begin we give a brief description of some of the magnetic features associated with stars along with an outline of the techniques, such as Zeeman-Doppler imaging that are used to observe such phenomenon.

We then move onto some of basic theory invloved in interpreting such phenomena and introduce some of the physics and calculations used to build the models. We give explanations on the methods used in extrapolating the coronal magnetic field from surface maps, calculating the pressure structure in the corona and determining prominence locations.

The young rapid rotator AB Dor is the first star to be disected. Due to the nature of Zeeman-Doppler imaging used to map a star's surface magnetic field, there is a lack of signature at the polar regions. We determine the effect on the global coronal structure of three current models for this polar field: that it is composed (a) of unipolar field, (b) of bipolar regions or (c) of nested rings of opposite polarity. We find only the presence of a unipolar spot has any significant effect on the overall coronal structure, forcing much of the polar field to be open.

We then move on to LQ Hya, and look at Zeeman-Doppler maps obtained from observations in Dec 2000 and 2001. We find a dynamic change in the coronal field structure over the one year period but with little change in the magnitude and rotational modulation of the X-ray emission.

Using the simpler magnetic field configuration of a dipole we look at the interaction of a star's open magnetic field with a planet. Observations of the system HD 179949 have shown repeated enhanced chromospheric emission that is synchronous with a planets orbital period. We investigate three factors that affect the variation of this emission.

Finally we look at variation of magnetic flux in comparison with the variation of the X-ray emission over a star's activity cycle. We look at three different models using magnetic maps produced from flux emergence and transport simulations. The results clearly show that although magnetic cyles may exist for stars they are not necessarily observable in the X-ray emission.

CONTENTS

LIST OF FIGURES

CHAPTER 1

Introduction

This chapter gives a brief description of some of the magnetic phenomena that are observed in the Sun with particular attention to magnetic sructures in the corona. We then introduce the subject of stellar magnetism for solar-like stars with emphasis on the coronal field structure and observable features such as X-ray emission. We also look at possible planet-stellar magnetic connections.

1.1 Solar magnetic activity

The magnetic fields found in and around stars are thought to be of two kinds. The first possibility, is that the magnetic field is a remnant of some past evolutionary stage. The second, and as in the case of the sun is that the magnetic field is believed to be amplified through a dynamo process, produced in a star's interior just below the convection zone, through the interaction of magnetic field with the differential rotation and turbulent convective motions (Parker, 1955).

Sunspots are possibly the most prominent magnetic feature observed on the Sun at the photosphere. The buoyancy of magnetic flux tubes created below the convection zone causes flux to rise up through the star's interior and emerge into the atmosphere. At the photosphere these strong concentrations of magnetic field inhibit convection making spots cooler than their surroundings and thus appear dark. In the case of the sun the magnetic field has a cyclic variation of approximately eleven years. This cyclic behaviour can be observed directly through the temporal behaviour of sunspots. At the beginning of a new solar cycle, sunspots tend to form at high latitudes, but as the cycle reaches a maximum (large numbers of sunspots) the spots form at lower latitudes. Near the minimum of

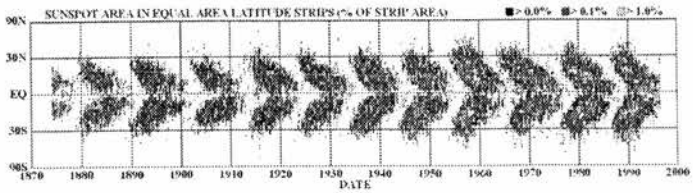

Figure 1.1: Position of sunspots from 1870 to 1995. Image courtesy of NASA

the cycle, sunspots appear even closer to the equator, and as a new cycle starts again, sunspots again appear at high latitudes. This recurrent behavior of sunspots gives rise to the "butterfly" pattern (Fig.1.1, and was first discovered by Edward Maunder in 1904.

Above the photosphere lies the chromosphere, a transparent region about 2500 kilometers thick. The chromosphere reveals its complicated network of supergranulation through obervations focused on the Ca II K emission line. Rising above the Sun's chromosphere we enter the transition region. This region is very narrow spanning only 30km and is mainly observed in EUV emission lines. Within the transition region the temperature jumps sharply from a few tens of thousands degrees Kelvin to as much as a few million degrees in the Sun's outer atmosphere. While the extreme temperatures in the solar corona are not fully understood, most heating mechanisms of the plasma are believed to be caused by various magnetic field phenomena. The coronal magnetic field is generally split into two opposing effects. The magnetic pressure which causes the plasma to expand versus the magnetic tension which traps the plasma. Tangling up of the magnetic field caused by the constant motion of field line footpoints at the photosphere can result in dramatic solar events such as flares, prominences and coronal mass ejections can be observed.

Other than at times of a solar eclipse the corona is not normally seen in white light. For more than 20 years now white light images of the solar corona have been collected using ground based K-coronameters such as the MK4 instrument at Mauna Loa, in Hawaii. These observations have been backed up more recently by satelite based coronagraphs such Skylab and SMM which reveal densities as high as $10^8 \mathrm{cm}^{-3}$.

X-ray observations are particularly suited to viewing the corona due to the extremely high temperatures. At these wavelengths the solar surface appears dark and a variety of structural features can be seen in the Sun's outermost atmosphere. We can split these features into two distinct groups of magnetic phenomena, open field and closed field. The first, appears relatively dark and are known as coronal holes; here field lines extend out

from the Sun providing channels for the plasma to flow along giving rise to a solar wind. The closed field regions refers to magnetic loop structures of which there is much variety of sizes, temperatures and densities (Bray et al., 1991). ranging from interconnecting loops that have densities of about $7 * 10^8 \mathrm{cm}^{-3}$ with temperatures of $2 * 10^6 K$ to compact flare loops with densities as high $\leq 10^{12} \mathrm{cm}^{-3}$ and temperatures exceeding $10^7 K$ (Orlando et al., 2004).

1.2 Stellar Magnetic activity

The changes in the Sun's magnetic field over its cycle are well known and have been studied for many years. In the case of solar-like stars however, observations of the surface distribution of flux are much more difficult to obtain. The technique of Doppler imaging allows us to map the surface brightness of rapidly rotating stars revealing spot patterns across the stellar disc. In contrast to what is observed on the Sun, these spots can be found at all latitudes, even up to the rotation pole (Strassmeier 1996). These observations have been explained by the emergence of flux tubes at high latitudes due to the strong Coriolis forces present in rapid rotators acting on the flux tubes in the convective interior (Schuessler & Solanki, 1992). While the distribution of spots may be very different to that on the Sun, in many cases the latitudinal differential rotation is surprisingly similar, even on stars rotating much more rapidly than the Sun (Donati & Collier Cameron, 1997).

Three possible models have been proposed to explain the latitudinal distribution of starspots. As early as 1992, Schuessler & Solanki (1992) proposed that flux tubes formed deep in the stellar convective zone would be deflected poleward by Coriolis forces as they attempted to rise buoyantly to the surface (Granzer et al., 2000). This would result in a polar cap that was formed of mixed polarity regions of a similar nature to those at lower latitudes. More recently, Schrijver & Title (2001) have presented a model for flux emergence on rapid rotators. A poleward meridional flow carries bipoles towards the poles while at the same time diffusion attempts to disperse them. The inclination of these bipoles to the equator causes the trailing polarities to reach the pole first, leading to a flux distribution which resembles concentric rings of alternating polarity encircling the pole. Finally, Kellett et al. (2002) have suggested on the basis of radio observations that the polar caps are formed of unipolar field, perhaps part of a large-scale dipole.

More complete information on the nature of stellar magnetic fields has become available with the advent of Zeeman-Doppler imaging (ZDI) This is a technique which uses high resolution circularly polarized spectra to map the magnetic flux distribution of rapidly rotating stars (Semel 1989). Stars that have been studied to date, AB Dor (P_{rot}=0.514 days), LQ Hya (P_{rot}=1.6 days) and the subgiant component of the RS CVn binary, HR1099 (P_{rot}=2.8 days), show patterns unlike that of the Sun with flux at all latitudes, and a strong azimuthal field that can form a uni-directional ring at high latitudes (Donati & Collier Cameron, 1997). Jardine et al. (2002a) have used maps obtained from Zeeman-Doppler images to extrapolate the coronal topology of the star AB Dor based on data acquired in 1995 Dec and 1996 Dec. This revealed that the large-scale field structure was dominated by a north-south arcade that extended right across the rotation pole. This arcade separated two large open field regions of opposite polarity centred at mid to low latitudes. This work assumed that the coronal field was potential. An extension of this to non-potential fields however, showed broadly the same field structure (Hussain et al., 2002). In turn Jardine et al. (2002b) followed this with a model of the X-ray emission of the star based on the extrapolated coronal field. This model reproduced the observed densities and the magnitude of the X-ray emission and showed that much of the X-ray emission would be expected to come from high latitudes where it would remain in view as the star rotated. Thus the X-ray emission would show very little rotational modulation. This is consistent with the BeppoSAX observation of two flares on AB Dor (Maggio et al., 2000) which showed no rotational self-eclipse of the flaring plasma during the flare decay phase which lasted for more than one rotation cycle.

The other single star for which maps of the surface magnetic field are available is LQ Hya. This star is similar in mass to AB Dor (1 $M_{\odot}$ for AB Dor and 0.95 $M_{\odot}$ for LQ Hya) and both stars are about 90 to 100 Myr old (Luhman et al., 2005). Both stars have a convective zone that is about 30% of the stellar radius (Kitchatinov et al., 2000). Where these stars do differ however is in their rotation rate, with AB Dor spinning 3.4 times faster than LQ Hya. In 1982 the star was found to be photometrically variable by Eggen (1984) and Fekel et al. (1986). Since then long term photometric studies have been carried out by Jetsu (1993) and Cutispoto et al. (2001). The observed variabilty of LQ Hya is caused by its magnetic activity which has been well established by the detection of widespread surface magnetic fields (Basri & Marcy, 1994; Donati & Collier Cameron, 1997). Photometric studies on LQ Hya show spotted regions to occupy up to 23% of the

total stellar surface (Alekseev & Kozlova, 2003). These studies have shown starspots to be localized at medium latitudes 24-48° confirming results from Doppler imaging which show the existence of medium latitude spots as well as near-polar starspots (Donati et al., 2003).

With the advent of ZDI, maps of the three vector components of the surface magnetic field became available. These showed yearly changes in the global field structure of LQ Hya, with significant changes (such as the polarity of the high-latitude azimuthal field) possible over the timescale of one year (Donati, 1999). Kitchatinov et al. (2000) presented a model for distributed dynamo activity on LQ Hya which reproduced many of these features and demonstrated that both axisymmetric and non-axisymmetric modes may be present, with the axisymmetric mode being favored. A similar result was found by Berdyugina et al. (2002) who analysed almost 20 years of photometric observations of LQ Hya. They found three possible cycle periods which may be associated with these different modes. They suggested that as stars spin down from their state of rapid rotation when very young, the dominant mode changes from non-axisymmetric to the axisymmetric form we find on the Sun. LQ Hya would represent some intermediate stage in this process.

1.3 X-ray observations

Yohkoh-SXT observations have shown that solar X-ray emission follows the Sun's 11 year magnetic cycle with a variation in amplitude of a factor of 30 (Stern et al., 2003). Suprisingly this is not common amongst other stars. ROSAT observations show the variation in X-ray emission for Sun-like stars to be only a factor of 2 or 3. Rather than assuming a Sun which is unique, Martens & SADE Team (2004) suggest that the Sun may belong to a small class of late-type stars that show large amplitudes in their X-ray cycles.

An investigation into the statistical variation of solar X-ray fluxes in the stellar context was carried out by Stern et al. (2003). The results suggest active stars may have very long or very weak cycles or no cycle at all. This suggestion is further complemented in the study by Micela & Marino (2003) where an analysis of the time variations of the solar X-ray luminosity is compared with other solar-like stars. The results show a fraction of moderately active stars to have an X-ray variability similiar to the Sun, while more active stars seem to lack solar-like cyclic activity. More recently results from the XMM-Newton

program have found large X-ray variability over a period of 2.5 years in the G2-type star HD81809 ($\nu \sin i = 3 kms^{-}1$). These results are the first direct observations of a solar-like star, other than the Sun, showing large amplitude modulation in the X-ray emission that is coherent with the activity cycle in the chromosphere (Favata et al., 2004).

If we look at more active stars, such as AB Dor, X-ray observations from Chandra and XMM-Newton paint a very different picture to that seen on the Sun (Dupree, 1993). Densities are in the region of $10^{10}\mathrm{cm}^{-3}$ and emission measures peak at 8 MK with an overall higher emission ($10^{52}\mathrm{cm}^{-3}$). Typical emission from an active region on the Sun peaks at $10^{52}\mathrm{cm}^{-3}$ at 2.5 MK (Brickhouse et al., 1995). In the case of AB Dor these high densities and emissions are associated with strong magnetic fields at the stellar surface. For rapidly rotating stars (AB Dor, $\mathrm{P_{rot}} = 0.514$ days), Zeeman-Doppler imaging confirms this connection by allowing us to measure the polarity distributions of stellar magnetic fields.

Long term photometric studies of AB Dor have suggested at least two activity cycles, firstly a 20 year cycle based on the variation of the mean brightness and secondly a flip-flop cycle whereby the dominant spot concentration shifts to another active longitude (Järvinen et al., 2005). Donati et al. (2003) however, hint at different activity cycles of 6-8 years due to the polarity switch of the poloidal component of the magnetic field. These observations also showed a distinctive lack of variation in the toroidal component of the magnetic field and thus estimates of any associated cycle would in the order of 14-16 years.

1.4 Planet-Stellar magnetic connections

More than 100 extrasolar planets have now been detected using high-resolution spectroscopic measurements. The methods employed such as Doppler and timing techniques (Mayor & Queloz, 1995; Marcy & Butler, 1998) provide basic information such as mass (orbital inclination dependent) and surface temperature estimates based on albedo. Most of these planets are regarded as large hot Jupiters with about 20% having orbital distances less than 0.1 AU.

Rubenstein & Schaefer (2000) and Cuntz et al. (2000) have suggested that stellar interaction of close-in extrasolar giant planets (CEGP's) could produce observable chromospheric emission on the parent star due to heating by magnetic reconnection events.

These ideas have been supported by observations of exoplanet systems such as HD 179949, υ And, HD 209458 and Tau Boo, where Shkolnik et al (2003) reported temporal variations in chromospheric emission of Ca II and K. In particular HD 179949 exhibited repeated enhanced emission synchronous with the 3.09-day planetary orbit inferred from radial-velocity observations (Shkolnik et al. 2003). The emission increases by 4%, peaking at phase $\phi = 0.83$ when the planet is approaching inferior conjunction (i.e when the planet is between the star and observer) and is least when the planet is near superior conjunction (i.e planet is behind the star). This modulation in the emission appeared to repeat consistently from 2001 August to 2002 August, a time interval of 108 orbits or 37 stellar rotations.

More recent observations of HD179949 by the same authors, however, show a reduced amplitude of modulation and a less well-defined phase lag from five data points secured in 2003 September (Shkolnik et al., 2004). These observations are consistent with a magnetic heating scenario. Tidal effects have been ruled out simply because there is only one signature per planetary rotation and not two (Shkolnik et al. 2003).

Following this work, Ip et al. (2004) constructed a simple model for the planetary magnetic field and showed that its interaction with a radial stellar magnetic field could produce a power output comparable with the magnitude of a typical solar flare. X-ray observations of solar flare events have shown that the energy release at the reconnection site at the top of the coronal loop creates a burst of electrons that accelerate down along the magnetic field lines until they impact on the stellar surface, evaporating chromospheric material. This in turn produces anomalous heating at the chromospheric layer. Ip et al. (2004) suggests that it is this type of effect that was observed at HD 179949 and υ And by Cuntz & Shkolnik (2002).

1.5 Summary

This thesis looks at the coronal field structure of young rapidly rotating solar-like stars. In particular we examine the large scale potential field structure of stars AB Dor and LQ Hya. We use magnetic maps obtained through Zeeman-Doppler imaging. With these maps we are able to extrapolate the coronal fields in order to determine locations of open and closed flux regions. By solving hydrostatic equilibrium along closed field lines we can

calculate, for an isothermal corona, the emission measure and emission measure-weighted density. These are quatities that can be compared with observations.

Further to this, we look at how the change in magnetic field throughout a young active star's cycle affects variability in its X-ray emission. Using surface maps produced from flux emergence simulations, we are able to determine properties of X-ray cycles that could be tested through observations.

Recent discoveries reveal what is believed to be the first indirect observation of an extra solar planet interacting with a star through a magnetic connection. We demonstrate the possible effects of different system geometries on the observable signature.

CHAPTER 2

Method

In this chapter we look at some of the basic theory invloved in calculating the structure of magnetic fields within a plasma. We also present some of the calculations that are common to the later chapters of this thesis.

2.1 Basic theory

Magnetohydrodynamics (MHD) is the theory of the macroscopic interaction of electrically conducting fluids with a magnetic field. The behaviour of such plasmas is governed by a continuity equation, an equation of motion, an energy equation and Maxwell's equations.

$$\frac{\partial \rho}{\partial t} + \nabla.(\rho \boldsymbol{\nu}) = 0 \tag{2.1}$$

$$\rho(\frac{\partial \boldsymbol{\nu}}{\partial t} + \boldsymbol{\nu}.\nabla\,\boldsymbol{\nu}) = -\nabla\, p + \boldsymbol{j} \times \boldsymbol{B} + \rho \boldsymbol{g_e} \tag{2.2}$$

$$\frac{\rho^\gamma}{\gamma - 1}\frac{D}{Dt}(\frac{p}{\rho^\gamma}) = -\mathcal{L} \tag{2.3}$$

$$p = \frac{k_B}{m}\rho T \tag{2.4}$$

$$\boldsymbol{j} = \frac{1}{\mu}\nabla \times \boldsymbol{B} \tag{2.5}$$

$$\nabla \times \boldsymbol{E} = -\frac{\partial \boldsymbol{B}}{\partial t} \tag{2.6}$$

$$\boldsymbol{j} = \sigma(\boldsymbol{E} + \boldsymbol{\nu} \times \boldsymbol{B} \tag{2.7}$$

$$\nabla.\boldsymbol{B} = 0 \tag{2.8}$$

$\boldsymbol{B}$ is the magnetic induction, ρ and p are the mass density and thermal pressure respectively. In stellar systems we are commonly dealing with velocities that are much less than

the speed of light and as such relativistic effects have not been considered in the above equations.

Using maxwell's equations we derive the more convienent and commonly used induction equation

$$\frac{\partial \boldsymbol{B}}{\partial t} = \nabla \times (\boldsymbol{\nu} \times \boldsymbol{B}) + \eta \nabla^2 \boldsymbol{B} \tag{2.9}$$

which determines the evolution of $\boldsymbol{B}$. The magnetic diffusivity η is assumed uniform. At this point it is worth taking into account the length scales that are involved in systems such as a stellar coronae as this can greatly simply the MHD equations. We define the magnetic Reynolds number as

$$R_m \equiv \frac{l_0 \nu_0}{\eta} \tag{2.10}$$

where l_0 and ν_0 are typical velocity and length scales of the system. This provides a measure of the strength of the coupling between the flow and the magnetic field. For stellar coronae in particular where length scales are the order of $10Mm$ $(10^7 m)$ and a typical velocity is $10^3 ms^{-1}$, $R_m \gg 1$. In such cases Ohm's law reduces to

$$0 = \boldsymbol{E} + \boldsymbol{\nu} \times \boldsymbol{B}. \tag{2.11}$$

We should note that currents are still present and are given by Eq.2.7. This condition is usually referred to as the perfectly conducting limit. Physically what this means is that the plasma behaves as if frozen to the magnetic field lines.

It is often the case that the MHD equations are greatly simplified and for the work presented in this thesis, we are mostly concerned with the static equilibria solutions $(\frac{\partial}{\partial t} = 0, \boldsymbol{\nu} = 0)$ of the MHD equations. We make this assumption based on the fact that much of the processes in plasma occur slowly, i.e on time-scales much longer than timescales the system in a stellar enviroment. Thus in the case where the sound speed $(\gamma p_0/\rho_0)^{1/2}$, the Alfv́en speed $B_0/(\mu\rho_0)^{1/2}$ and the gravitational free-fall speed $(2gl_o)^{1/2}$ are all much larger than the flow speed the equation of motion (Eq.2.2) can be characterized by magnetohydrostatic balance

$$-\nabla p + \boldsymbol{j} \times \boldsymbol{B} + \rho \boldsymbol{g_e} = 0. \tag{2.12}$$

2.2 Extrapolating the coronal field

We write the magnetic field $\boldsymbol{B}$ in term of a flux function Ψ such that $\boldsymbol{B} = -\boldsymbol{\nabla}\Psi$ and the condition that the field is potential ($\boldsymbol{\nabla} \times \boldsymbol{B} = 0$) is satisfied automatically. The condition that the field is divergence-free then reduces to Laplace's equation $\boldsymbol{\nabla}^2\Psi = 0$. A solution in terms of spherical harmonics can then be found:

$$\Psi = \sum_{l=1}^{N} \sum_{m=-l}^{l} [a_{lm} r^{l} + b_{lm} r^{-(l+1)}] P_{lm}(\theta) e^{im\phi}, \tag{2.13}$$

where the associated Legendre functions are denoted by P_{lm}.

$$B_r = -\sum_{l=1}^{N} \sum_{m=-l}^{l} [l a_{lm} r^{l-1} - (l+1) b_{lm} r^{-(l+2)}] P_{lm}(\theta) e^{im\phi} \tag{2.14}$$

$$B_\theta = -\sum_{l=1}^{N} \sum_{m=-l}^{l} [a_{lm} r^{l-1} + b_{lm} r^{-(l+2)}] \frac{d}{d\theta} P_{lm}(\theta) e^{im\phi} \tag{2.15}$$

$$B_\phi = -\sum_{l=1}^{N} \sum_{m=-l}^{l} [a_{lm} r^{l-1} + b_{lm} r^{-(l+2)}] \frac{P_{lm}(\theta)}{sin\theta} ime^{im\phi} \tag{2.16}$$

The coefficients a_{lm} and b_{lm} are determined by imposing the radial field at the surface from the Zeeman-Doppler maps and assuming that at some height R_s above the surface the field becomes radial. The source surface model crudely simulates the effect of the closed coronal field opening up into the solar wind. For the active star AB Dor, the presence of large slingshot prominences observed around the co-rotation radius which lies at $2.7R_\star$ from the rotation axis leads us to believe that much of the corona is closed out to those heights and so we set the value of R_s to $3.4R_\star$. In order to calculate the field we used a code originally developed by van Ballegooijen et al. (1998) to study the formation of filament channels on the sun. The value chosen for N depends on the particular surface magnetograms we are studying. For AB Dor we set $N = 63$ which corresponds to a resolution of 1.4° at the equator on the stllar surface. This more than matches the surface resolution of surface magnetograms obtained through Zeeman-Doppler imaging. In the case of LQ Hya we can reduce N to 31 as the resolution of surface magnetograms for this star is much less.

We would like to note that the potential field model is an approximation of the true stellar field. Hussain et al. (2002) fitted a non-potential field to the observed Stokes profiles. They found the field structure to be similar to the potential model at all low

to mid latitudes. At high latitudes the potential model was less accurate. This is due to concentration of electric currents in the polar regions that require a non-potential description of the field.

2.3 Calculating the position of prominences

Once we have extrapolated the coronal field we can then calculate the position of stable potential minima along field lines based on the numerical method set out by Pointer et al. (2002). For a possible prominence formation site to exist the component of effective gravity along the magnetic field must be zero, i.e. $\boldsymbol{B}.\boldsymbol{g_{eff}} = 0$. For this position of equilibrium to be stable we also require it to be a potential minimum. Thus the equilibrium must satisfy the condition

$$(\boldsymbol{B}.\nabla)(\boldsymbol{B}.\boldsymbol{g_{eff}}) < 0. \tag{2.17}$$

Such stable points may be favoured positions for prominence formation as any gas condensing at this point would neither fall towards the surface nor be centrifugally expelled. The fact that prominences on AB Dor are observed around the co rotation radius suggests that such minima in the gravitational-centrifugal potential do have a role to play in determining where prominences form. The existence of such stable points does not however guarantee prominence formation. In fact, at distances as far out as the co rotation radius, the curvature of the field lines would need to be much smaller in order to overcome the centrifugal acceleration acting on a prominence. Prominences are observed as transient H_α absorption features and so can only be seen when they occult the stellar disk. We therefore select out of all possible stable points those that transit in front of the disk. Hence due to the stellar inclination any points that will transit the disk must satisfy the condition

$$R\cos(\theta + 60) < 1 \tag{2.18}$$

where R is the radial height of the stable point and θ is the latitude. If a star has a purely dipolar field, all such stable points would lie in the equatorial plane. If like AB Dor or LQ Hya the star has an inclination of 60° the prominences would be unobservable (Jardine et al., 2001).

2.4 X-ray emission

The X-ray emission is determined from the closed field regions in the corona. First of all the pressure structure of the corona is calculated assuming it to be isothermal and in hydrostatic equilibrium. Thus the pressure at any point is

$$p = p_0 e^{\frac{m}{kT}\int g_s ds} \tag{2.19}$$

where $g_s = (\mathbf{g}.\mathbf{B})/|\mathbf{B}|$ is the component of gravity along the field and

$$\mathbf{g}(r,\theta) = \left(-GM_\star/r^2 + \omega^2 r\sin^2\theta, \omega^2 r\sin\theta\cos\theta\right), \tag{2.20}$$

with ω the stellar rotation rate. The plasma pressure is scaled to the magnetic pressure at the loop footpoints i.e. $p = KB_0{}^2$ where the constant of proportionality K is chosen to match observed emission measures for rapidly rotating solar like star's such as AB Dor (Sanz-Forcada et al., 2003b). The models presented here have used temperatures of $10^7 K$ and $10^6 K$ for the corona. These temperatures are chosen based on observations of active stars where the peaks in the X-ray luminosity are found to be in this temperature region. Observations of the active star AB Dor show the peaks in the X-ray luminosity to be at $10^{6.8} K$ and $10^{7.3} K$ (Linsky & Gagne (2001)). As we move out to larger heights from the star the gas pressure is greater than the magnetic pressure and thus forces field lines to open up. We have included this effect in our model by setting the plasma pressure to zero wherever it is greater than the magnetic pressure i.e. where $\beta > 1$.

For short timescale effects on the field such as coronal mass ejections we would see supersonic velocities for the gas flow which would certainly have a strong effect on the structure of the field. A potential field model however represents the lowest energy configuration for the magnetic field and as such does not allow any such reconnection events. Flows like stellar winds could still result in the bending of open field lines for this model. The flows required to significantly bend the field lines would need to be supersonic. Since we are concerned with a corona closed out to heights of $2.5R_{star}$, which lies well below the sonic point, we have ignored any effect that the ionized gas flow might have on the field structure.

From the pressure, the coronal density is calculated assuming it to be an ideal gas (eqn.2.4). Using a Monte Carlo radiative transfer code we can then determine the X-ray emission as a function of the radial field at the surface.

CHAPTER 3

Polar fields for AB Dor

In all of these scenarios, the polar caps would appear dark in a Doppler image if the polar fields were strong enough to suppress convection. What these Doppler images cannot reveal is whether the polar field is composed of closed loop structures which may be bright in X-rays, or open field regions which may contribute to the sellar wind. This question becomes of importance when considering the processes of angular momentum loss in a stellar wind, which has traditionally been modelled on the basis of an aligned dipole field where most of the open (wind-bearing) field lines emerge from near the stellar pole. It is also relevant to studies of disk magnetosphere interaction and channeled accretion flows in young stars.

3.1 AB Doradus

We take as our example star the young rapid rotator AB Doradus which has been studied in depth for the last decade or so. Surface brightness maps have been collected annually since 1988 (Collier-Cameron & Unruh, 1994; Unruh et al., 1995; Collier Cameron, 1995). In the last seven years Zeeman-Doppler maps of the surface magnetic field have been secured on an annual basis. Long term studies of the star's X-ray variability have shown a small rotational modulation (5-13 %) and a large emission measure of $10^{52-53}\mathrm{cm}^{-3}$ (Vilhu et al., 1993). This implies that AB Dor has either a very extended or very dense corona. AB Dor has an inclination of 60° and therefore much information about the lower hemisphere is lost. In the upper hemisphere however, the pole remains in view constantly and X-ray emission from high latitudes would therefore suffer little rotational modulation. BeppoSax observed a flare (Maggio et al., 2000) that showed no rotational modulation over a period

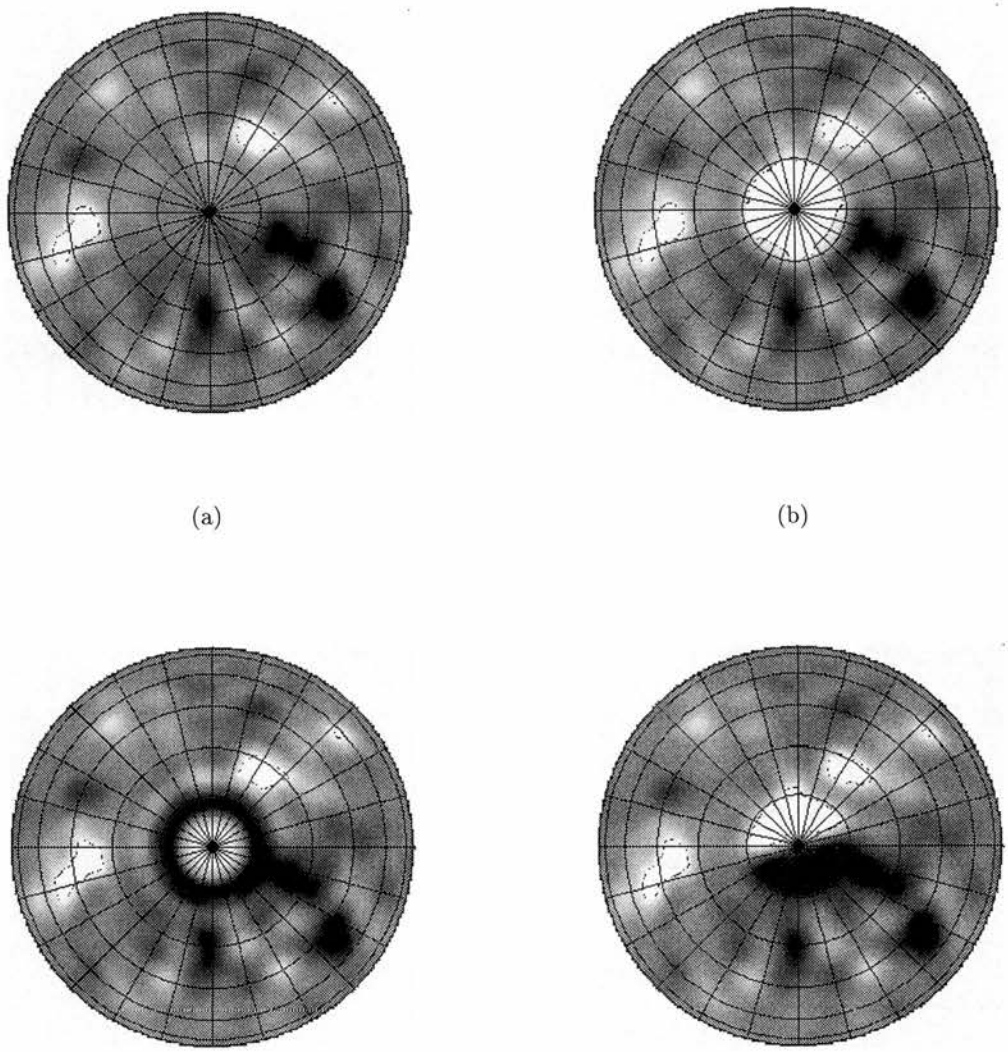

(a) (b)

(c) (d)

Figure 3.1: Surface maps of the magnetic field for AB Dor for Dec 1995 shown from a viewpoint looking down on the rotation pole. Fig.1a shows the surface magnetic field as it is observed with no field added to the polar region. Fig.1b has a large unipolar spot, Fig.1c, has concentric rings of opposite polarity and Fig.1d, has a bipolar configuration. The strength of the field added to each model is 1kG.

greater than the rotation period of the star. Modelling of the flare decay showed that the flaring loops must be small and hence must be situated at latitudes above 60° in order to remain in view.

Complementary to these observations are spectroscopic studies of the star's X-ray emission from which the thermal structure, abundance stratification, and densities of the corona can be investigated. Recent studies with XMM showed coronal densities to be extremely high ranging from $3 \times 10^{10}\mathrm{cm}^{-3}$ (Güdel et al., 2001) to $10^{12}\mathrm{cm}^{-3}$. This high density immediately suggests that the emitting loops would be relatively small and compact. If this is the case, to explain the lack of rotational modulation, these loops would have to be located at latitudes high enough to remain in view as the star rotates. High latitude magnetic loops are consistent with Doppler images of AB Dor where we can see dark polar spots along with spots at lower latitudes. Zeeman-Doppler images show magnetic flux to be present all over the surface of AB Dor apart from at the poles where the surface brightness is so low that the Zeeman signal is suppressed (Donati & Collier Cameron, 1997).

Any model applied for the field at the pole will have to explain the lack of rotational modulation in the X-ray emission as well as being consistent with the observations of large prominences that form preferentially at or just beyond the Keplerian co-rotation radius, which for AB Dor is at 2.7 stellar radii from the rotation axis (Collier Cameron & Robinson, 1989a,b). As many as six prominences may be present at any one time in the observable hemisphere of the star. Since they co-rotate with the star, they must be held in place by the coronal magnetic field. This suggests that at least some fraction of the coronal field is in the form of closed loops even at these large distances.

The structure of the large scale coronal magnetic field of AB Dor was investigated by Jardine et al. (2002a). They took the surface magnetic field determined from Zeeman-Doppler imaging and extrapolated it into the corona, assuming it to be potential. They found that the closed field regions of the corona extended over the polar regions. By filling the corona with isothermal plasma in hydrostatic equilibrium, they determined the spatial distribution of the coronal X-ray emission (Jardine et al., 2002b). Much of this emission came from high-latitude regions where it was never rotationally self-eclipsed. This naturally gave a low rotational modulation in X-rays, similar to the observed value. The derived magnitude of the emission measure and the emission-measure weighted mean

density were also consistent with observations. Jardine *et al*also explored the effect on the X-ray emission of adding in a global dipole and determined that because this would cause the polar regions to be open (and hence dark in X-rays) this could not be reconciled with the BeppoSAX flare observations that suggest the presence of closed loops at high latitudes (Maggio et al., 2000).

In this chapter, we consider the impact of some alternative models that may explain the dark polar caps. Rather than a global dipole which extends over the whole surface, we consider a single unipolar spot at the pole which covers a limited surface area. We also consider two possibilities for mixed-polarity regions at the pole: either a single bipole or concentric rings of alternating polarity. These configurations were added to the poles of the 1995-1996 mixed map of AB Dor. In each case the global field was extrapolated and the positions of stable points which are possible prominence formation sites and the X-ray emission were determined. The effects on these properties were examined for different strengths of polar field ranging from 500G to 2000G. Below this upper limit, polar fields would escape detection. Although the polar areas on AB Dor are dark and the Zeeman signal is thus suppressed, Donati & Collier Cameron (1997)have shown that if the polar region was to have a field in excess of a few thousand Gauss there would be some signal of the polar field detected by Zeeman-Doppler imaging.

3.2 Results

The magnetic fields added to the star are depicted in Fig.1 as is the original surface field map. All three additional fields have a strength of 1kG. This is a reasonable estimate for the field at the pole as it is strong enough to suppress convection yet not so strong as to be detectable in the star's Zeeman-Doppler images.

As can be seen in Fig.2, where we have shown only those field lines that are anchored at points within the polar region in question, the unipolar spot model has the greatest effect on the global field topology. Closed loops from the polar region are forced down to lower latitudes due to the presence of strong open field at the pole. This is unlike the other two models with the concentric rings and bipole, which show a strikingly similar appearance to the original data set of having large closed loops crossing directly over the pole. In these models there is almost no open field emerging from the polar region.

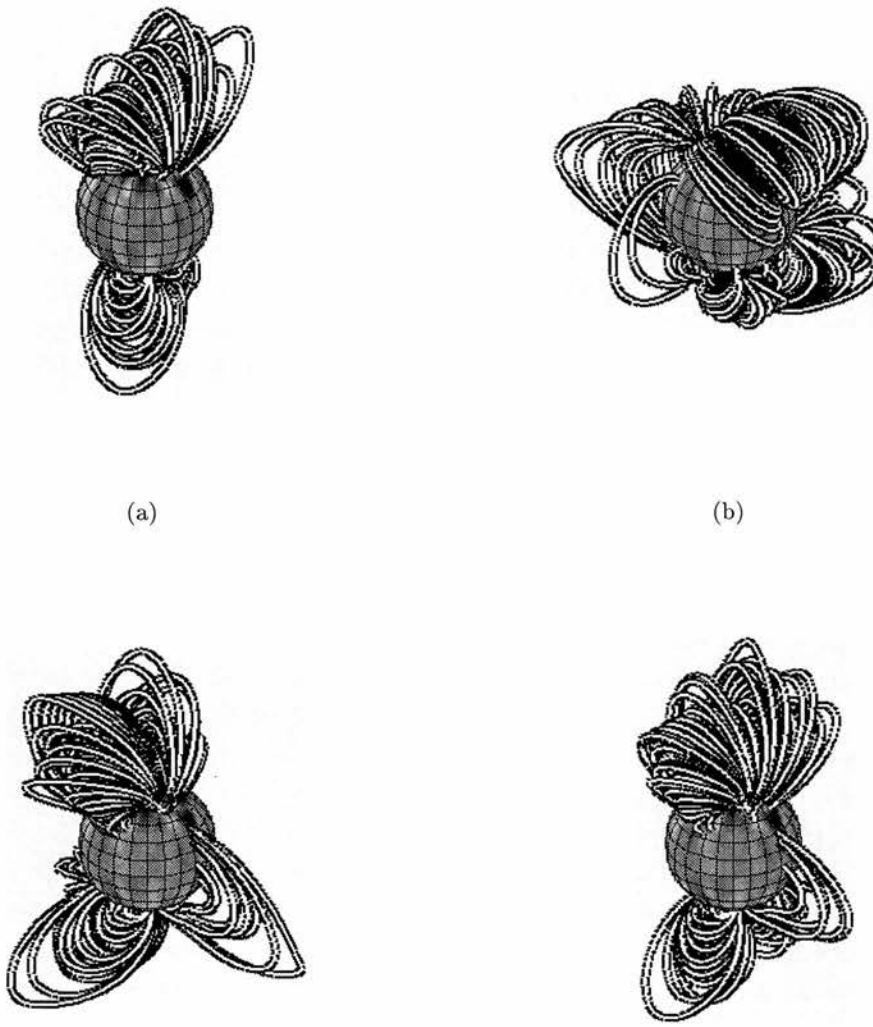

(a) (b)

(c) (d)

Figure 3.2: Closed field emerging only from the polar regions where we have added flux. Strong similarities can be seen between the original image, concentric rings and bipole models. In these cases the field lines from the polar region connect primarily to the surface at high latitudes. Only in the case of a unipolar spot (b) do the field lines connect to the rest of the stellar surface.

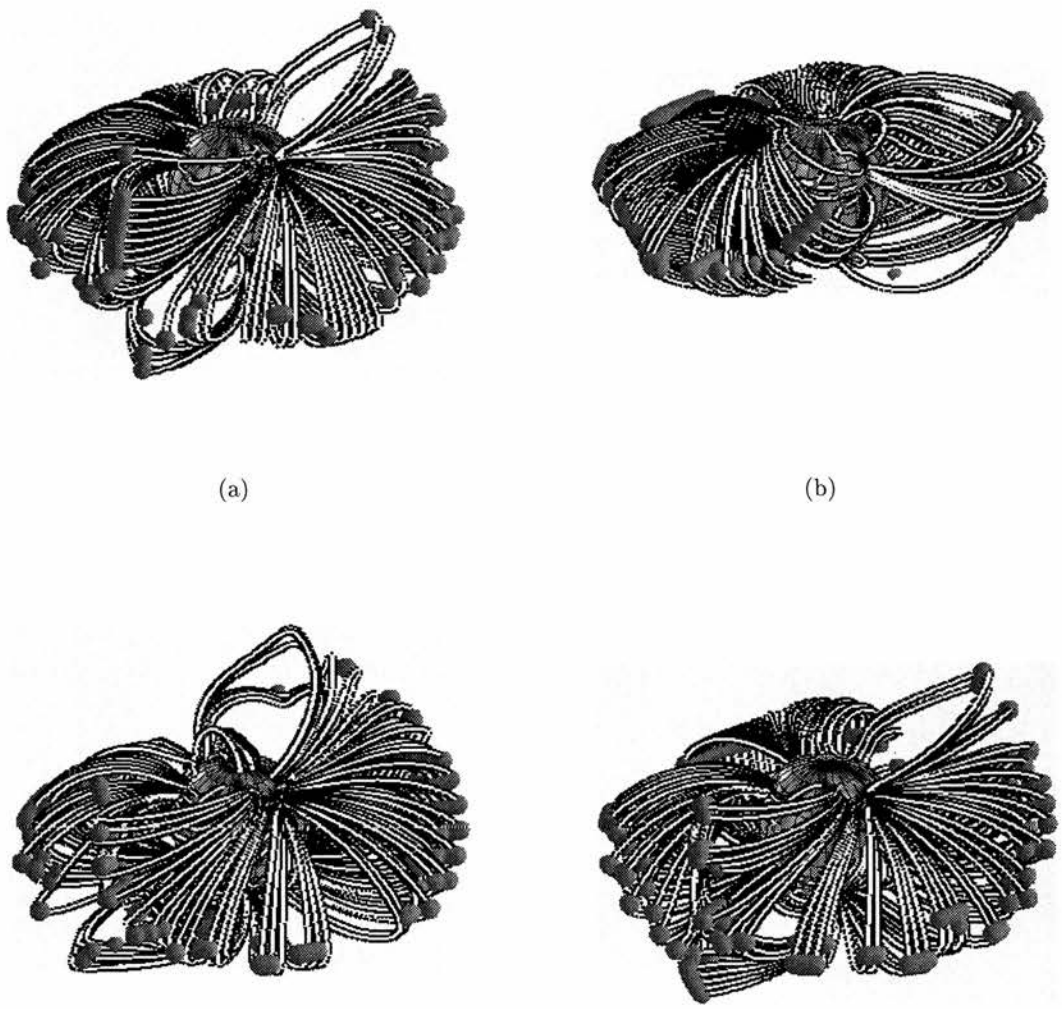

(a) (b)

(c) (d)

Figure 3.3: Surfaces with closed field lines show possible locations of prominences.At each of these points the effective gravity along the field line is zero and the point lies at a potential minimum. Moving from top left to bottom right, polar conconfigurations considered are: nothing at the pole(a), global dipole(b), concentric rings(c), bipole at the pole(d). Each polar cap added has field strengths of 1kG.

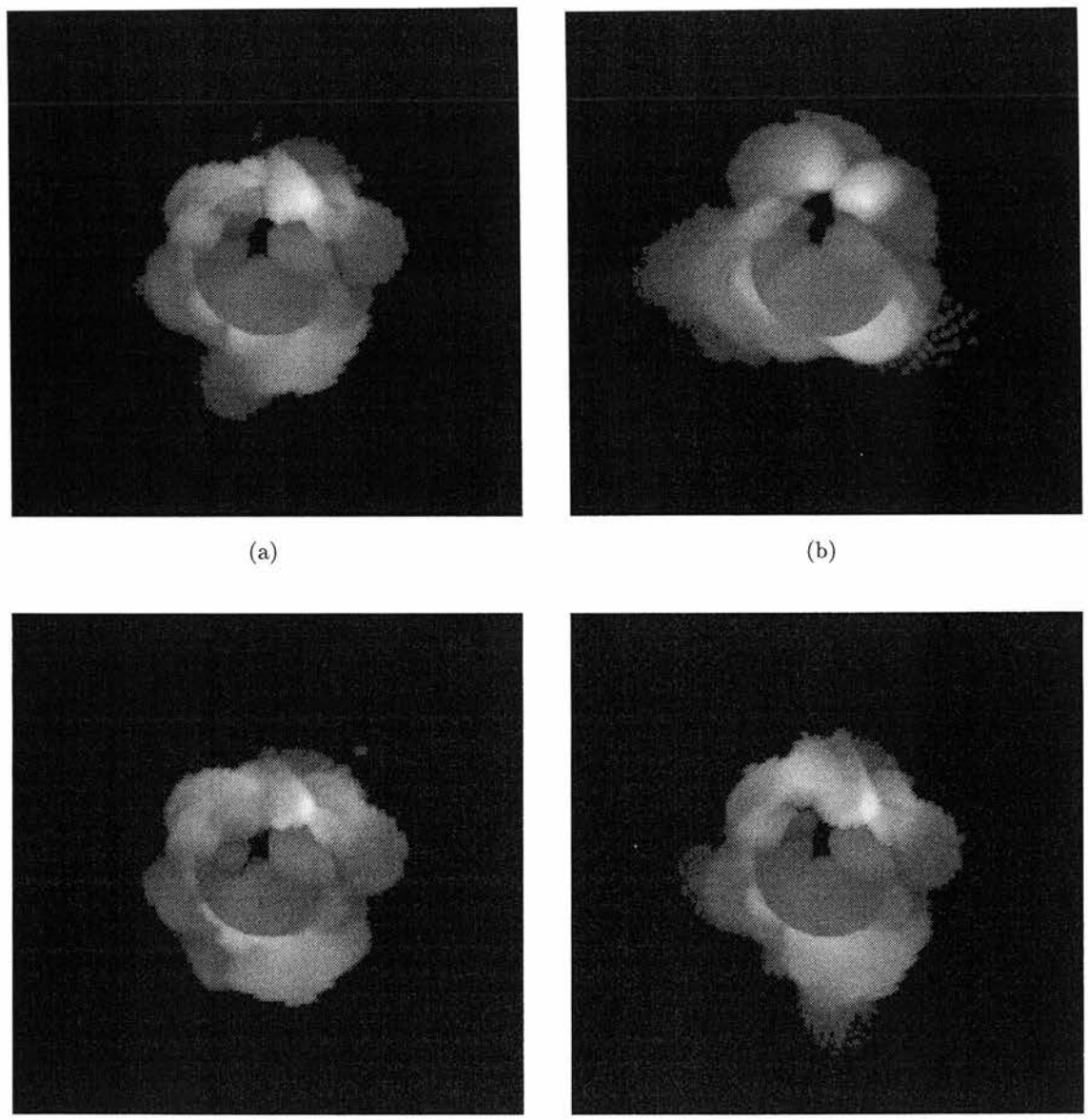

(a) (b)

(c) (d)

Figure 3.4: X-ray images of the stellar corona for each model. Same layout as previous figures. The X-ray emissions are all calculated for a coronal temperature T=10^7K.

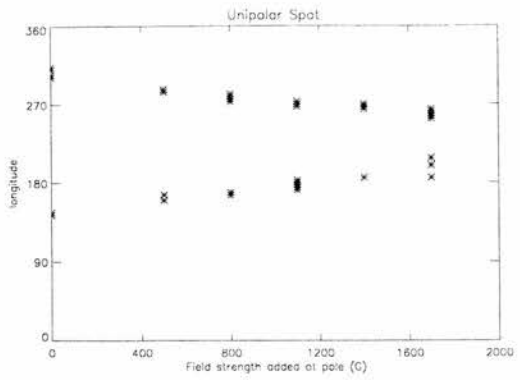

(a)

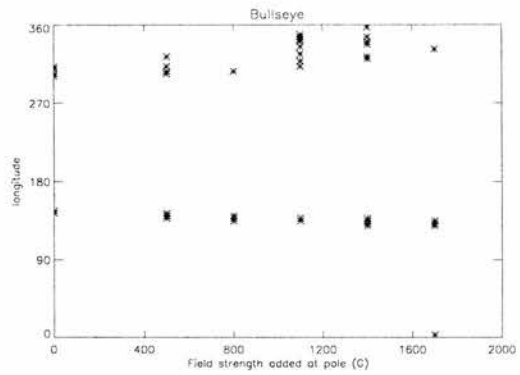

(b)

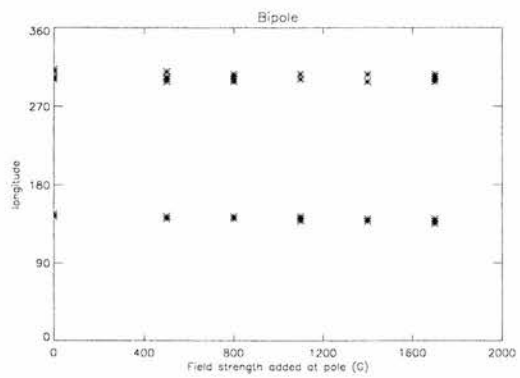

(c)

Figure 3.5: The graphs above show the longitude for stable points where possible prominces may form and would pass in front of the star so they may be detected. The results here are fairly conclusive showing that all three models have roughly two regions of longitude where prominences could be detected.

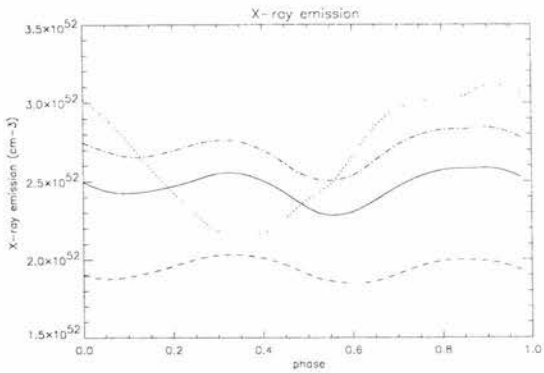

Figure 3.6: Graph showing the X-ray emission measure as it varies with phase for each model. All models here do not differ too much in magnitude and certainly the original data(solid line), concentric rings(dashed line) and Bipole(dash-dots) show a remarkably similar curve in emission over a whole cycle. This is also reflected in their rotational modulation which shows little variation between these three models and fits into the range of values predicted by observations of 5-13%. The Unipolar spot model (dotted line) shows a much higher rotational modulation of 31.52%.

The concentric rings and bipole models show greater consistancy in the lack of rotational modulation of the flaring X-ray emission seen in BeppoSAX observation.

The difference in the topology of the field that is added at the pole can be seen in Fig (3.7) which shows the fraction of the surface flux that is open. In the case of a single unipolar spot added to the pole, this fraction increases as the strength of the polar field is increased, reaching a maximum value of 15%. This is less than the corresponding value of 44% for a dipolar field with the same source surface imposed (Jardine et al., 2002a) but still represents a significant factor. The open field regions extend down to a latitude of 75° with the result that much of the polar regions would be dark in X-rays. For the other two types of polar field, however, most of the polar field lines are closed (see Fig (3.2)) and so very few of them contribute to the flux of open field. In this case, the fraction of open field decreases as the polar field strength increases. This is due to the field at the pole being able to connect locally.

Positions of possible prominences are less affected by the addition of a polar field. Again the unipolar spot has the greatest effect forcing the stable points toward the equatorial plane of the star (Fig.3). Many of these points which lie in or near the equatorial plane cannot be observed crossing the star along our line of sight. Observations of prominences

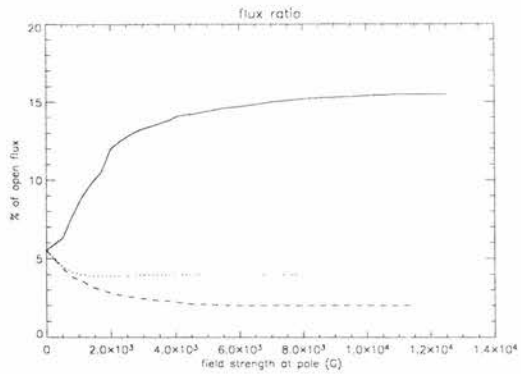

Figure 3.7: The graph shows the change in the amount of open magnetic flux as we increase the field strength at the poles of the various models. Any flux that reaches the source surface is considered open hence we calculate the amount of open flux as a ratio of total flux emerging at the stellar surface: $\sum_A |B_r(R_s, \theta, \phi)| / \sum_A |B_r(R_*, \theta, \phi)|$ The solid line shows the change for the unipolar spot model, the dotted line represents the concentric rings model and the dashed line the bipolar model. Again the similarities between the concentric rings and bipole models is easily seen, both slowly decreasing in open flux as we increase the strength of the polar field. The unipolar spot model on the other hand shows a reasonable growth in open flux with increasing field strength at the poles. It should be noted that although we have shown the flux ratios for magnetic fields up to 12kG these fields are much too strong to be considered non-detectable and are only shown to display the saturation each of the models has on the open flux.

are possible only if the prominences transit our line of sight to the star causing absorption dips in the Hα profile. Strangely however the number of stable points for the dipole model is not that much less than any of the other models, although there does seem to be some convergence of longitudes as we increase the field strength at the pole for this model. The concentric rings and bipole models reproduce the same pattern of sites as the original image. In all three models we find that the stable points are grouped into two regions where arcades of predominantly east-west field span a range of longitudes.The imposition of the polar field disturbs the summits of these structures, pushing them toward longitude 220° in the unipolar case, and away from longitude 220° in the concentric case.

Clearly, none of these models can fully explain the number of prominences that are observed (up to six in the observable hemisphere at any one time). One possibility is that these stable points are not reliable indicators of prominence formation sites. Alternatively, as suggested by Schrijver & Title (2001) it could be that the prominences are formed in the sheared field produced when differential rotation stretches out the unipolar field of the dark polar cap to produce an azimuthal field. Such fields have been observed on AB Dor for some time (Donati & Collier Cameron, 1997). Recently, Hussain et al. (2002) have fitted non-potential magnetic fields to the observed Stokes profiles. They have shown that the currents (which mark the regions where the field departs from its lowest-energy state) are confined to the high latitude regions at the edge of the dark polar cap. The positions of the stable points in these field extrapolations, however, were not significantly different from those determined for a potential field.

Pointer et al. (2002) performed a potential field extrapolation from a Zeeman-Doppler image of AB Dor with a dipolar field added into the map. They showed that differential rotation acting on such a field would produce a high latitude ring of azimuthal field similar to that observed (Donati & Collier Cameron, 1997). It is possible that the field produced by the flux emergence model of Schrijver & Title (2001)would have a similar effect. Here the differential rotation between the concentric rings of opposite polarity would shear the field crossing this boundary producing an azimuthal field. A third possibility is that, as suggested by Hussain et al. (2002), the closed corona is in fact confined to within $1.6R_\star$ and the prominences are confined in the very cusps of helmet streamers, much further out than the rest of the corona.

The other observable quantity is the X-ray emission. This was calculated for each

model with polar fields of 1kG. Looking at the X-ray images of the stellar corona (Fig.4) for each model it is clear that the original image, the concentric rings and bipole models all show a strong similarity with a predominant X-ray emission from the polar region. The unipolar spot does show some emission from the polar region although not nearly as much structure as the other models. The average emission measure did not vary significantly between the models, ranging from $1.9\times10^{52}\mathrm{cm}^{-3}$ for the concentric rings to $2.73\times10^{52}\mathrm{cm}^{-3}$ for the bipole. The unipolar spot model has the highest emission measure with a value of $3\times10^{52}\mathrm{cm}^{-3}$ but it has such a large rotational modulation (31.5%) that its average emission lies at $2.61\times10^{52}\mathrm{cm}^{-3}$. The other models all show a level of rotational modulation (9 to 11%) that fits the values predicted by observations of 5 to 13% (Kuerster et al., 1997). Something else worth noting here is that the models, excluding the unipolar spot, all showed very similar X-ray light curves. This again strongly suggests that the presence of a mixed-polarity field at the pole has little effect on the overall structure of the star.

3.3 Conclusions

Using Zeeman-Doppler images of the surface magnetic field of the young, rapidly rotating dwarf AB Dor, we have investigated the effect on the coronal field structure of the three most popular models for the polar fields of young stars. We find that the addition of a mixed-polarity region at the pole results in more small-scale local flux tubes at the pole, but has little effect on the large-scale field structure. Consequently, observations of the magnitude or rotational modulation of the X-ray emission are not sufficient to discriminate between these types of models. Observations of the "slingshot prominences" trapped in the coronae of these stars do not provide an observational discriminant either. We have determined possible prominence-bearing structures by calculating the sites of stable mechanical equilibrium. All three models showed no more than 2 structures that can transit the stellar disc, but the observations show condensations at all longitudes. Due to the nature of alternating magnetic polarity at the surface of the star it is thought that a helmet streamer model could provide us with more regions of longitude for possible prominence formation sites where each prominence site would lie above and between these regions of opposite polarity (Linker et al., 2001).

The large-scale field structure is affected rather more by the addition of a unipolar

region at the pole. This forces more of the polar field lines to be open (and hence dark in X-rays). This gives a larger rotational modulation as the closed-field regions that are bright in X-rays are now at lower latitudes and so are subject to rotational self-eclipse.

A polar spot extending down to latitude 75° gives a rotational modulation of 31.5%, greater than the observed value of 5-13% (Kuerster et al., 1997). It also forces up to 15% of the flux that emerges through the surface to be open, compared to only 5% when no field is added at the pole. This has potential implications for the angular momentum lost in the stellar wind, not only because it changes the amount of open flux, but also because it affects the distribution in latitudes. The addition of a polar spot introduces many more high-latitude open field lines. The winds from high latitude regions remove significantly less angular momentum from the star because of the reduced lever arm of the fieldlines. Schuessler & Solanki (1992) showed that this may explain the apparent slow-down of the angular momentum loss in young rapid rotators.

The change in the global field structure brought about by adding a polar spot may also be relevant to studies of disk-magnetosphere coupling in young stars. The addition of a polar spot means that the largest scale field lines (the ones that would intersect a disk) originate from the poles. In this case, any material accreting from a disk would reach the stellar surface at the poles. In the absence of a polar spot (or in the case where the polar field was of mixed polarity) the accretion process would be more likely to be in the form of discrete accretion funnels, which would intersect the stellar surface in low-latitude 'hot spots'.

While the nature of the polar field - whether single or mixed polarity - clearly makes a difference to the global field structure, the available observations of the X-ray emission measure and the prominence distribution are not sufficient to discriminate between types of polar field. We can however rule out the posibility of the unipolar spot model because the results show the modulation amplitude in the X-ray emission to be much too large. Only the degree of modulation of the X-ray emission can be used, but this requires long-term monitoring to eliminate the effects of short-term variablity in flares. Phase-resolved observations of line shifts that indicate the presence of a stellar wind would perhaps be a good proof of the field structure, but it may be that it will only be with the advent of Zeeman-Doppler imaging in molecular lines that we will be able to determine the nature of the polar fields.

CHAPTER 4

The changing corona of LQ Hya

This chapter aims of to examine the large-scale potential field structure of LQ Hya, in order to determine the locations of the open and closed flux regions. The nature of the global field is not only of interest from the point of view of field generation by a dynamo, but also to the whole question of stellar spin down. Open field lines that are rooted close to the stellar rotation pole provide less efficient wind losses than lower-latitude flux (Solanki et al., 1997). Over the course of its cycle, the open flux of the Sun changes its location from being mainly polar at cycle minimum (when the global field is closest to a dipole) to emerging from much lower latitudes at cycle maximum (Lockwood, 2003; Wang et al., 2002; Mackay et al., 2002) when higher-order non-axisymmmetric modes become apparent. By solving hydrostatic equilibrium along the closed field lines we can calculate, for an isothermal corona, the emission measure and the emission measure-weighted density. These are the two quantities that can be compared with observations. We focus particularly on the changes that are apparent in the data from Dec 2000 and Dec 2001. These maps were reconstructed with very dense phase coverage and so provide a reliable image of the surface flux.

4.1 Modelling the corona of LQ Hya

We note that since LQ Hya is inclined at approximately 60° to the observer, only one hemisphere can be imaged reliably. Zeeman-Doppler imaging produces flux values for all parts of the stellar surface, becoming progressively less reliable below latitudes of -30°. The effect of this "missing flux" on the global field topology was investigated by Jardine et al. (2002a) for the case of AB Dor which has a similar inclination. They created an

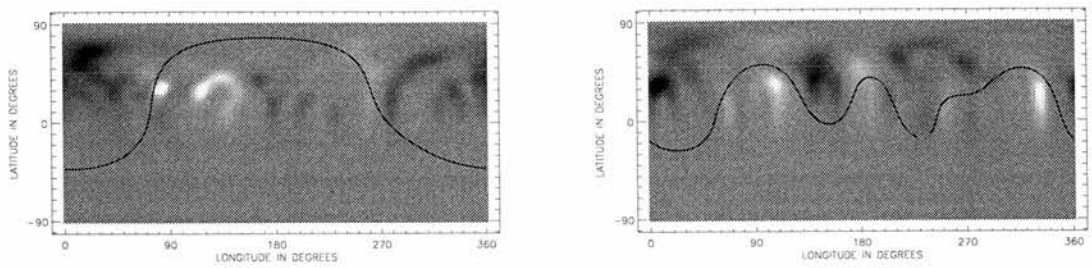

(a) (b)

Figure 4.1: Radial field maps at the surface of LQ Hya for years (a) Dec 2000 and (b) Dec 2001. The black line represents the neutral polarity at a height of $2R_\star$. White represents +500G, while black represents -500G.

artificial surface map in which the map from Dec 1995 forms one hemisphere and the map from Dec 1996 forms the other. They concluded that the nature of the lower-hemisphere flux did indeed affect the topology of the low-latitude field, where field lines connected across the equator, but that the mid- to high-latitude field topology was unaffected. For the work presented here we are more interested in the change in field structure from one year to the next and have chosen to ignore the effect of the invisible part of the stellar surface.

For a given coronal temperature this model has two free parameters: the radius of the source surface which determines the magnetic field structure and the constant K which scales the coronal pressure and density. K was set to a value of 10^{-5} in order to give an emission measure consistent with observations (Sanz-Forcada et al., 2003a). In the previous models of AB Dor's corona (Jardine et al., 2002a) the source surface was chosen to be at about 3.4 stellar radii. The reason for this is that large slingshot prominences are observed mainly around the co-rotation radius which lies at $2.7R_\star$ indicating that much of the corona is closed out to these heights. In the case of LQ Hya the choice of source surface seems more arbitrary due to the lack of observable phenomena. We can obtain an upper limit on the source surface by determining, for a dipolar field, the point at which the ratio β of the plasma pressure to the magnetic pressure reaches unity. To do this we take the simplest solution of (1), which is a dipole aligned with the rotation axis with $l = 1$ and $m = 0$ and impose the boundary conditions

$$B_r(r = R_\star) = 2M \cos\theta / R^3 \tag{4.1}$$

$$B_\theta(r = R_s) = 0 \tag{4.2}$$

where $M = B_r(r = R_\star, \theta = 0)R_\star^3/2$ is the dipole moment . Choosing a dipole field to find the height where β reaches unity ensures that for all other higher order terms in the spherical harmonic expansion, $\beta < 1$ since for all these terms the magnetic field drops off faster with radial distance.

A test height was deliberately over estimated at 6R$_\star$. By selecting out a closed field line that stretches out to this test height, the change in the ratio β along this field line could be followed. We find that, for a base pressure of 1 Pa, a temperature of $10^7 K$ and a field strength at the pole of 400 G, β rises rapidly with distance from the stellar surface reaching unity around $r = 2.5R_\star$. Placing the test height further out (say to $10R_\star$) has little effect on the height at which $\beta = 1$. Dropping the temperature to $2 \times 10^6 K$ has a much more dramatic effect, pushing the height where $\beta = 1$ to about $r = 4.7R_\star$. Dropping the base pressure to 0.01 Pa at this temperature pushes the β point out even further, close to the Keplerian co-rotation radius that lies at about $6R_\star$. It seems that a slight variation of the parameters can have a considerable effect as to where β will reach unity. For this study we are going to choose the source surface to be at $r = 2.5R_\star$. This gives good agreement with observations of the emission measure by Sanz-Forcada et al. (2003a). Later in this chapter we discuss the implications that moving the source surface has on the X-ray emission and open flux which in turn is linked to the amount of angular momentum loss of the star.

4.2 Changes in magnetic topology

The changes in the surface magnetic field of LQ Hya from 2000 to 2001 have already been described by Donati et al. (2003) who noted the growth of the higher order modes with time. This can be seen clearly in the radial field maps shown in Fig.1a and Fig.2b by noting the structure of the neutral polarity contour. In 2000, the surface map shows that one set of longitudes (from 80° to 270°) were of predominantly negative polarity, while the others were of positive polarity. This is very similar to the global field structure for AB Dor and results in a large north-south arcade running over the pole (Fig.2a). Clearly, in the spherical harmonic decomposition of equation (??) the m=1 mode must be strong. One year later, however, the field structure has changed. The neutral polarity contour shows

(a) (b)

Figure 4.2: Closed field regions for LQ Hya calculated from Zeeman-Doppler maps in (a) Dec 2000 and (b) Dec 2001. The image is viewed from a longitude of 180° and a latitude of 30° consistent with the stellar inclination of 60°. Note that because of the stellar inclination only the upper hemisphere is totally in view and so can be imaged reliably. We have therefore plotted only fieldlines in this hemisphere. The surface radial maps are painted onto the stellar surface in each case.

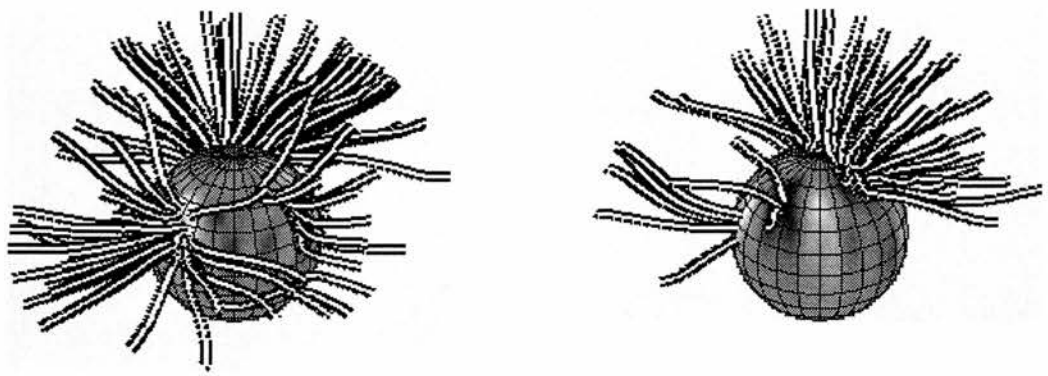

(a) (b)

Figure 4.3: Open field regions for LQ Hya calculated from Zeeman-Doppler maps in (a) Dec 2000 and (b) Dec 2001. As in Fig.2a and Fig.2b we have plotted only upper-hemisphere field lines. The surface radial maps are painted onto the stellar surface in each case.

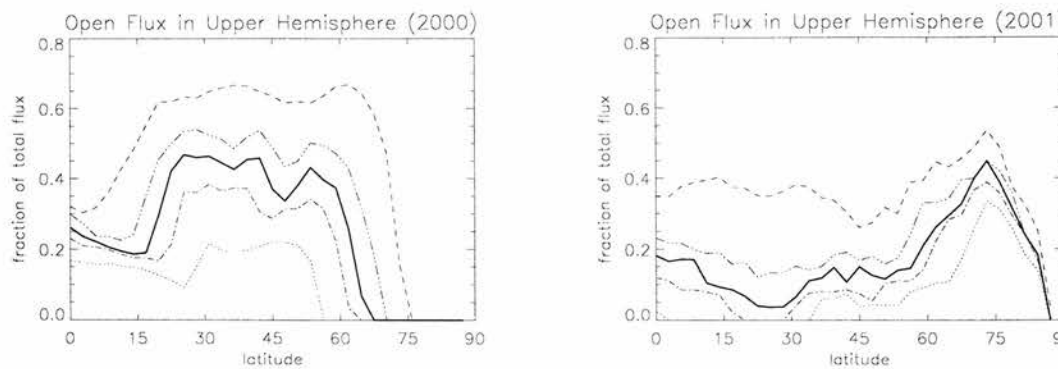

(a) (b)

Figure 4.4: The fraction of the total flux that is open as a function of latitude in (a) Dec 2000 and (b) Dec 2001. Different line styles denote different source surface radii: $R_{ss}/R_{\star}$ =1.5 (dashed), 2.0 (dash dot-dot-dot), 2.5 (solid), 3.4 (dash-dot) and 5.8 (dotted) which is approximately the Keplerian co-rotation radius for LQ Hya. While the fractional contribution of the open flux to the total flux increases as the source surface moves closer to the stellar surface, the distribution with latitude is qualitatively unchanged. There is a significant difference however between the distributions in 2000 and 2001, with the peak of the distribution moving to much higher latitudes in 2001.

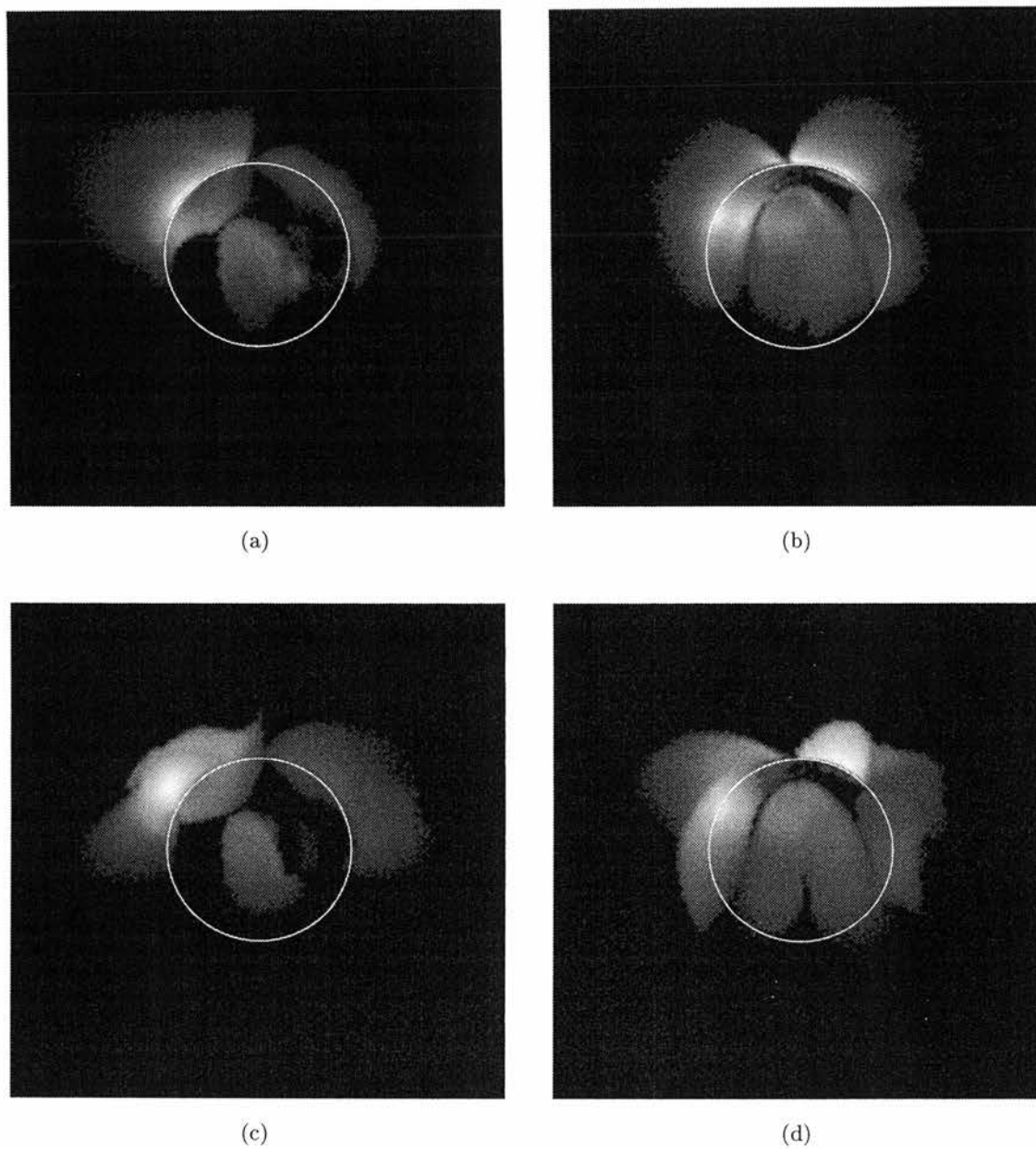

(a) (b)

(c) (d)

Figure 4.5: X-ray images of the stellar corona for the two years. (a) and (c) are Dec 2000 while (b) and (d) are Dec 2001. The images shown here are for X-ray emissions calculated for a coronal temperature of 10^6K (top) and 10^7K (bottom). We can see how much more extended the emitting region of the corona is in the 10^7K model than the 10^6K. Surprisingly there is little change in the emission measure between the two years despite obvious structural changes in the corona. The white circle superimposed on the images represents the stellar disc.

a more complex structure, with many more changes of polarity along a line of latitude. This results in a more complex global field structure, with many more north-south arcades (Fig.2b). Clearly, modes of higher m-value have been excited (Donati, 1999). Although AB Dor has been observed on an almost yearly basis, such a dramatic change in the magnetic topology has not been seen (Jardine et al., 2002a).

To see this change in context, we can compare it to changes in the Sun's magnetic field over the course of its cycle. At cycle minimum, the field most closely resembles an aligned dipole with most of the open field emerging from the polar regions. As the cycle progresses and more east-west bipoles emerge, the higher-order modes become stronger and the coronal holes (which contain the large open field regions) extend down from the poles towards lower latitudes. While on small scales this behaviour is very complex, on the largest scales a simpler pattern emerges. The changes in the heliospheric field can simply be described as a dipole that is aligned with the rotation axis at cycle minimum, but rotates down into the equatorial plane at maximum (Smith et al., 2003).

These changes in the Sun's large-scale field have been studied both observationally and theoretically (Lockwood et al., 1999; Solanki et al., 2002). The contribution to the total field of the axisymmetric (or aligned) dipole and the non-axisymmetric (or tilted) dipole over the cycle have received much attention (Wang et al., 2000; Mackay et al., 2002). We define the total contribution of flux from the aligned dipole component ($l = 1, m = 0$) at the stellar surface as

$$\Psi_{10}(R_\star) = \int \Psi_{10}(R_\star, \theta, \phi) d\Omega / 4\pi \tag{4.3}$$

and the tilted dipole component ($l = 1, m = 1$)

$$\Psi_{11}(R_\star) = \int |\Psi_{11}(R_\star, \theta, \phi)| d\Omega / 4\pi. \tag{4.4}$$

Mackay et al. (2002) used a model of flux emergence and transport to study the behaviour of the solar field over many cycles. They looked in particular at the evolution of the first two modes from this expansion for full solar cycle simulations. It was found that the flux from the aligned dipole component (Ψ_{10}) increased as the flux from the tilted dipole (Ψ_{11}) decreased with this latter component reaching a maximum at solar maximum.

This simple sinusoidal pattern for the Sun's cycle is not what we see for LQ Hya. At first sight, LQ Hya shifts from a dominant tilted dipole in 2000 ($\Psi_{10}/\Psi_{11} = 0.7$) to a strong aligned dipole field in 2001 ($\Psi_{10}/\Psi_{11} = 4.3$). This explains the open field structure we can

see in Fig.3a and Fig.3b but does not explain the abundance of closed east-west field that is seen in Fig.2b. This field is related to the strength of the higher modes from the spherical harmonic expansion. On inspection of the higher order modes we find that (l=3,m=3) is the strongest mode in the spherical harmonic expansion in 2001 and contributes nearly twice that of the aligned dipole mode to the overall flux function (1). This mode is directly responsible for the arcades of loops we see in this year (Fig.2b). This is a very different picture from what we see on the Sun where the higher harmonic modes never dominate over the north-south axisymmetric dipole or the east-west non-axisymmetric dipole. We can see open flux is spread across mid latitudes in 2000 (Fig.3a) with little flux near the pole. In contrast, Fig.3b shows the open field to be mostly concentrated around the polar region. Zeeman-Doppler images of the polar regions in both 2000 and 2001 show weak signal at the pole, despite the obvious large spot found in brightness maps (Donati et al., 2003). It is therefore possible that the large change in structure of the open field could be overemphasized due to the missing flux at the poles. McIvor et al. (2003) however, showed that for the similar dwarf star AB Dor, the presence of polar field had almost no noticeable effect on the global coronal field structure. In one case, where a unipolar spot was placed at the pole, the coronal field was influenced but this model was ruled out due to the extremely large x-ray modulation values. The location and amount of open field at the surface will have strong implications for the stellar wind and hence the angular momentum loss. Due to the short lever arm of the field lines at high latitudes there is significantly less angular momentum lost in these winds (Solanki et al., 1997). Fig.4 shows the change in open flux with latitude. Ignoring the southern hemisphere where very little Zeeman signal could be detected, we can clearly see a shift in the latitude where the open flux is strongest between the years 2000 and 2001.

The effect of changing the position of the source surface from the value of $2.5R_\star$ used elsewhere in this chapter can also be seen. Moving the source surface closer to the star increases the amount of open flux, but has little effect on its distribution with latitude.

4.3 Changes in X-ray emission measure and density

The X-ray images Fig.4.5 which are determined from the closed field regions also exhibit an obvious change in the structure. Observations based on a single rotation cannot distinguish

between a transient X-ray brightening (flare) and the rotational modulation of a quiescent stable structure. Hence detecting such a change from year to year would require long term monitoring such as the five year ROSAT observations of AB Dor (Kuerster et al., 1997). Unfortunately, unlike AB Dor, this modulation in X-ray emission is not available for LQ Hya as yet. Despite obvious changes in the structure of the magnetic field from one year to the next, the models show little difference in the total emission measure. The observed total emission measures for LQ Hya are $10^{49.8}\mathrm{cm}^{-3}$ for 10^6K and $10^{51.15}\mathrm{cm}^{-3}$ for 10^7K (Sanz-Forcada et al., 2003a). For the models shown in Fig.5.4 this corresponds to densities $10^{9.4}\mathrm{cm}^{-3}$ and $10^{9.8}\mathrm{cm}^{-3}$ for 10^6K and 10^7K respectively. For the models at 10^6K a small variation in emission between the years could be seen but it would most likely be undetectable in observations. In both years at 10^7K the corresponding densities were almost indistinguishable. It should be noted that values of emission at 10^6K as quoted from Sanz-Forcada et al. (2003a) are uncertain due to the few lines that occur in the temperature region. Looking at similar stars where there are more lines at this temperature however does paint a general picture of the emission at 10^6K being somewhat less that at 10^7K. Due to the way we observe the X-ray emission from a star it is not possible to differentiate between the emission from flares and the emission in the quiescence. It has been proposed (Maggio et al., 2000) that the observed emission which corresponds to these high densities could be due to the continuous presence of flares. This is far from what we observe on the Sun but flaring has been detected through X-ray emission and in some cases for the entire duration of one rotation period of the star (Maggio et al., 2000).

The densities here are far higher than that of the Sun but are close to that observed for the similar star AB Dor where line ratios indicate densities of $10^{10.8}\mathrm{cm}^{-3}$ (Sanz-Forcada et al., 2003b). For LQ Hya, similar line ratios at 10^7K indicate densities greater than $10^{12}\mathrm{cm}^{-3}$ (Sanz-Forcada et al., 2003a). Such high densities do not agree with current loop models where it is believed that any loops forming in regions with such high gas pressure would be blown open and hence not contribute towards the star's X-ray emission. For models used here densities as high as this would result in a reduction of the emission measure as we can see in Fig.5.4 where the emission for the 10^7K models falls off below the 10^6K models at higher densities. Imposing a cutoff in the emission when the plasma pressure exceeds the magnetic pressure causes a reduction in the emission measure at higher densities due to the emitting volume of the corona shrinking.

For the models of years 2000 and 2001 the rotational modulation showed little change

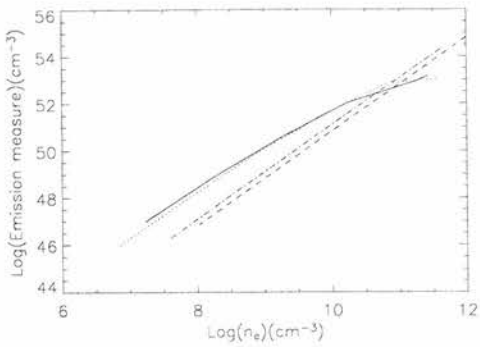

Figure 4.6: Total emission measure as a function of the emission measure weighted coronal density for a source surface at 2.5$R_\star$. Models for the year 2000 at 10^7K (solid) and 10^6K (dashed) as well as for the 2001 at 10^7K (dotted) and 10^6K (dash-dot) are shown. The reduction in the emission measure for very high densities is due to the plasma pressure exceeding the magnetic pressure and forcing field lines to open.

between the two years despite the obvious change in the global field structure. In 2000 the rotational modulation at 10^7K was calculated to be 21% and in 2001 26%. The corona is much more confined at 10^6K due to the effect of temperature on the density scale height. This causes a drop in the overall emission measure but increases the rotational modulation. At this temperature there was almost no difference from year to year in the modulation with values of 44% for both years. These values were not noticeably effected by changes in density. In both years we are seeing a relatively high modulation. For the 10^6K model this is easily explained by the fact that the emitting region is much more compact due to the higher densities and as such is self-eclipsed as the star rotates. At 10^7K the reduction in modulation compared to the 10^6K model is because of higher latitude emitting regions that remain in view for longer periods of time as the star rotates.

This result is reflected in the distribution of open flux, an important feature when we come to consider the rate of loss of angular momentum. In 2001 where we have a marginally higher modulation this is accompanied by more open field at higher latitudes which does not contribute to the X-ray emission. The dominance of the higher order mode in the spherical harmonics expansion (l=3,m=3) plays an important role in the balance of the X-ray modulation from one year to the next. If the dipole mode was the dominating mode this year then there would be a greater amount of open flux at the pole and would most likely extend further down in latitude. Due to the inclination of this star, this would decrease the amount of closed flux that would remain constantly in view and thus the

rotational modulation would increase.

4.4 Choice of Source surface

The effects of the source surface must be considered. The potential field extrapolation for these models is partly determined by the choice of source surface which is simply an artificial boundary to help us calculate the structure of the coronal field. We choose this boundary based upon the fact that at some height above the star the field will open up due to the magnetic pressure being overpowered by the gas pressure i.e. $\beta > 1$. As can be seen from Fig.4.4 the overall amount of open flux does depend on the choice of source surface but there seems to be little effect to the distribution in latitude. It would have been possible to calculate the emission measure for a range of densities and source surfaces and then compare these to the observed densities and emission measures to obtain a choice of source surface based on real observations. The emission measure, however, is fairly insensitive to the choice of source surface as is the density. Only for source surfaces less than $1.5R_\star$ is a drop seen in the emission measure. This clearly shows that most of the X-ray emitting corona is confined close to the stellar surface. Moving the source surface further out also increases the coronal volume where we have $\beta > 1$. The potential field extrapolation does not account for this and any closed field lines that lie in a region where $\beta > 1$ are likely to be unphysical as they would be blown open by the gas pressure.

4.5 Conclusions

Using the Zeeman-Doppler images to calculate the coronal magnetic field of LQ Hya we have shown that the structure of the global magnetic field has changed considerably over the space of one year and this is clearly illustrated in both the closed field (Fig.2a and Fig.2b) and open field topologies (Fig.3a and Fig.3b). In 2000, the large-scale field resembled a tilted dipole, with the open field emerging at low to mid latitudes. One year later the open field is mainly at pole and the large scale field more closely resembles an aligned dipole, albeit with a significant contribution from higher-order modes.

This significant and obvious change in the structure is very different from that of the Sun. On the largest scales, the Sun's magnetic field does indeed show a gradual change

over its cycle, from being mainly an aligned dipole at cycle minimum to more like a tilted dipole at cycle maximum (Smith et al., 2003). On the Sun, however, the growth of the higher-order modes signals the transition from minimum, where there are few east-west bipoles, to cycle maximum, where there are many bipoles. A strong contribution from higher order modes is therefore associated with the phase of its cycle when the large scale field most closely resembles a tilted dipole. This is just the opposite of what we see on LQ Hya.

The change in the distribution and magnitude of the open flux seen in the models over the two years is an interesting feature when we consider the star's loss of angular momentum. On making the simple assumption that more angular momentum will be lost from field lines nearer the equator than at the pole, due to the larger lever arm, we would expect to see a drop in the angular momentum lost over the two years. Without more information on the nature of the magnetic cycle, however, it is impossible to determine the extent to which the changing latitude of the open field regions will influence the angular momentum loss.

Intriguingly, even although the field structure changes significantly in the course of one year, the densities and emission measures that we derive are very similar, as is the rotational modulation in X-rays. At temperatures of 10^7K, the emission measures of $10^{49.8}$cm^{-3} for 10^6K and $10^{51.15}$cm^{-3} for 10^7K are consistent with the observed values although the derived densities of $10^{9.4}$cm^{-3} and $10^{9.8}$cm^{-3} are somewhat lower (Sanz-Forcada et al., 2003a). This suggests that X-ray observations alone are not sufficient to provide detailed information on coronal structure. With the advent of new polarimeters (such as ESPADONS on the CFHT) however, our ability to produce Zeeman-Doppler images of stars will be greatly enhanced.

CHAPTER 5

Simulated X-ray cycles

The aim of this chapter is to show how the change in magnetic field throughout a young active star's cycle affects the variability in its X-ray emission. It is clear from Zeeman-Doppler observations that rapidly rotating solar-like stars such as AB Dor exhibit low and high latitude spots of mixed polarity (Strassmeier, 1996). It is this observation that led Mackay et al. (2004) to show, using magnetic flux emergence and transport simulations, that the intermingling of magnetic polarities in the polar regions of active stars is possible. In these simulations it was found that an increased meridional flow and changes to the butterfly diagram, such as emergence of bipoles at higher latitudes, were required to reproduce the observed high latitude fields of AB Dor.

At present, there are no direct observations of magnetic cycles on young solar like stars. Using the simulated surface maps that best describe the observable features seen on AB Dor we extrapolate the coronal magnetic field an hence calculate the X-ray emission assuming an isothermal corona. By using the simulated surface maps we are able to determine properties of X-ray cycles that could be tested through observations. We also choose to look at variations in the magnetic flux, in particuliar, the change in latitude of the open flux throughout the cycle. The location of open flux has strong implications for the mass loss and loss of angular momentum for a star.

5.1 Simulated input data

We consider three sets of surface maps over the period of 11 years produced by the flux emergence simulations of Mackay et al. (2004). Each of these maps showed good intermingling of magnetic polarities at high latitudes due to the increased region of flux emergence

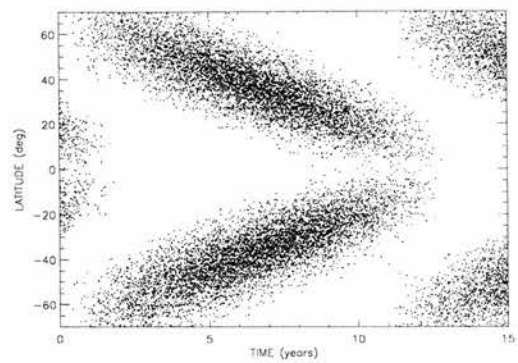

(a)

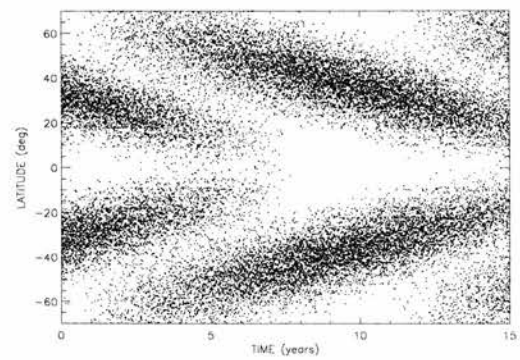

(b)

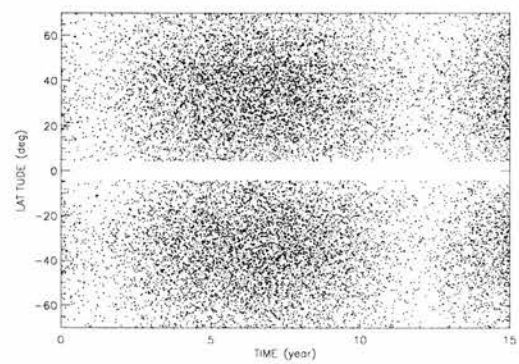

(c)

Figure 5.1: Input data for the simulations. (a) butterfly pattern (b) overlapping butterfly and (c) no butterfly pattern. In all three cases the region of flux emergence extends up to 70°.

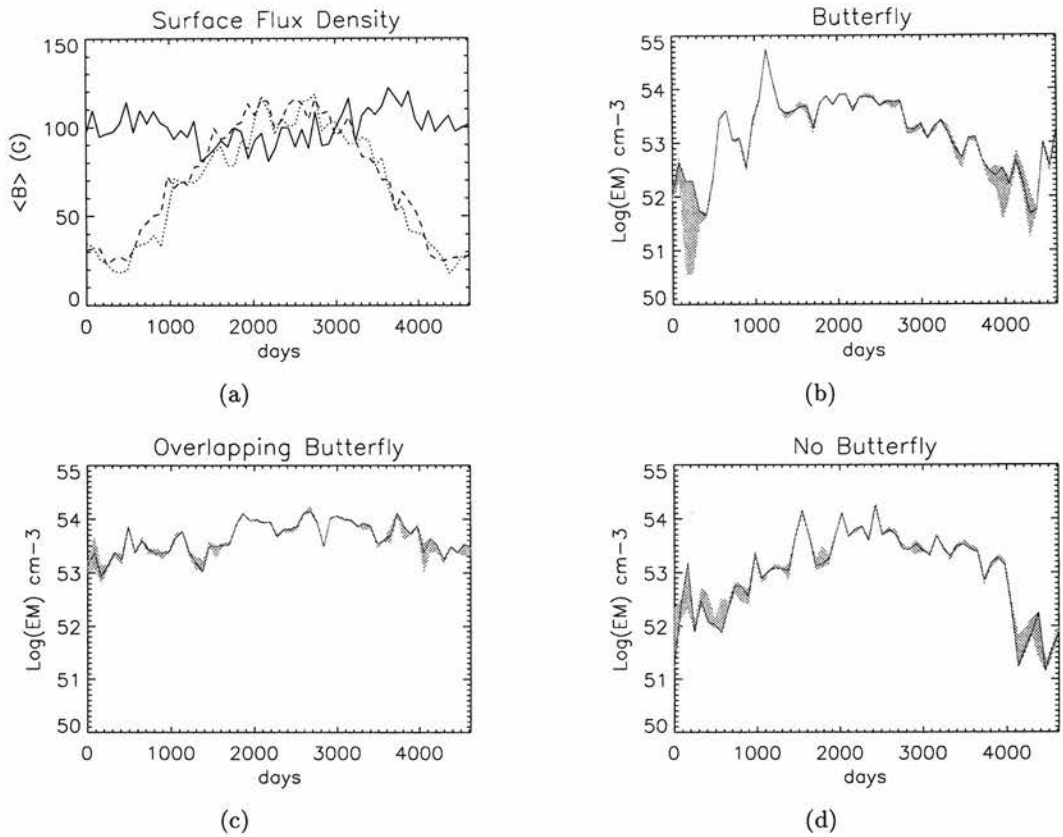

Figure 5.2: (a) The variation of the average surface magnetic field ($\Phi_{tot}(t)/4\pi R_\star^2$) over the course of a cycle. The solid line represents the overlapping butterfly, the dotted line is the butterfly and the dashed line is the model with no butterfly pattern. Figures (b), (c) and (d) show the variation in X-ray emission over the cycle. Figure (b) shows the case where the butterfly pattern was used, (c) shows the case where the butterfly overlaps and (d) no butterfly. Shaded areas correspond to maximum and minimum values of emission due to the rotational modulation and the solid line represents the average X-ray emission within one stellar rotation.

and increased meridional flows. Emerging flux at higher latitudes is appropriate for active stars, where the faster rotation rates lead to a strong Coriolis force which in turn causes a poleward drift of the emerging magnetic field (Schuessler & Solanki, 1992). The first data set represents a butterfly diagram much like that observed on the Sun but with the region of flux emergence increased up to 70° (Fig.5.1(a)). In this case both the latitude at which the magnetic flux appears and the amount of flux vary over the cycle. At cycle minimum most of the emerging flux is at high latitudes (at the start of the cycle) or at low latitudes (at the end of the cycle). At cycle maximum (when the total surface flux is greatest) most of the bipoles, and hence presumably most of the X-ray bright regions, are at mid latitudes. The second set of surface maps is the same as the first except that the butterfly pattern overlaps by 4 years (Fig.5.1(b)). This overlap results in a total surface flux that in contrast to the first dataset is almost constant through the cycle (see Fig.5.2(a)). At cycle minimum the flux is spread over a range of latitudes as the high latitude contribution from one wing of the butterfly overlaps with the low-latitude contribution from another wing. At cycle maximum however, the flux is mainly at mid-latitudes. The third set of surface maps has no butterfly pattern but still has an extended region of emergence (Fig.5.1(c)). In this case we have removed the latitudinal variation of the surface flux over the cycle, but left the variation in the total amount flux (see Fig.5.2(a)). These are the three models out of the study by Mackay et al. (2004) that reproduce the pattern of mixed polarity regions observed on active stars. They allow us to investigate the effect on the X-ray emission of not only the magnitude of the surface magnetic flux but also its distribution in latitude throughout the cycle.

5.2 calculations

Using the methods outlined in chapter 2 we extrapolate the coronal magnetic field and calculate emission measures for the simulated surface maps of Mackay et al. (2004).

Using the surface maps we also calculate the total flux $\Phi_{tot}(t)$ and the total open flux $\Phi_{open}(t)$ based on the magnitudes of the radial field B_r and open radial field $B_{r(open)}$ at the surface.

$$\Phi_{tot}(t) = R_\star^2 \int |B_r(R_\star, \theta, \phi, t)| d\Omega \tag{5.1}$$

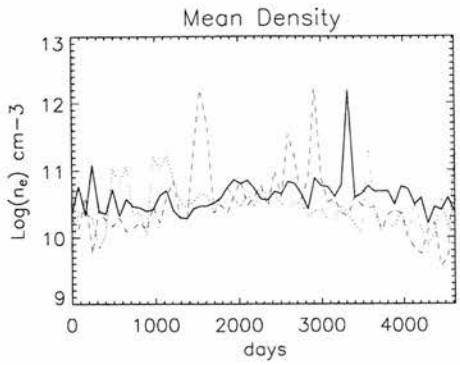

Figure 5.3: The variation of the mean density for each model throughout the cycle. The solid line represents the overlapping butterfly, the dotted line is the butterfly and the dashed line is the model with no butterfly pattern.

$$\Phi_{open}(t) = R_\star^2 \int |B_{r(open)}(R_\star, \theta, \phi, t)| d\Omega \tag{5.2}$$

5.3 Results

5.3.1 X-ray emission

The total magnetic flux of the butterfly and no-butterfly models can be seen to vary by more than a factor of 4 over the 11 year cycle Fig.5.2(a). The overlapping butterfly model however, shows little change, and remains at a roughly constant level of flux over the cycle. This is as expected, if we consider what is happening in terms of the emerging bipoles, the overlapping butterfly has a consistent level of flux as when activity in one cycle decreases it increases in the other keeping the level of flux approximately constant .

The X-ray emission (Figs.5.2(d),5.2(c),5.2(b)) shows similiar features to that seen in the total surface flux. Both the butterfly and no-butterfly models show a variation in the X-ray emission that spans 2 orders of magnitude. The overlapping butterfly model, again, shows no cyclic variation in the X-ray emission over the 11 years. We should note however, that the peak in emission over a cycle is of the same order of magitude in all three cases. It is a dip in the emission we see for the butterfly and no-butterfly models during cycle minimum rather than a peak at cycle maximum. The associated mean density for each model is plotted in Fig.5.2. The densities for all three models are typically in the range of 10^{10} to $10^{11} cm^{-3}$. This is in good agreement with the value of $10^{10.5} cm^{-3}$ obtained

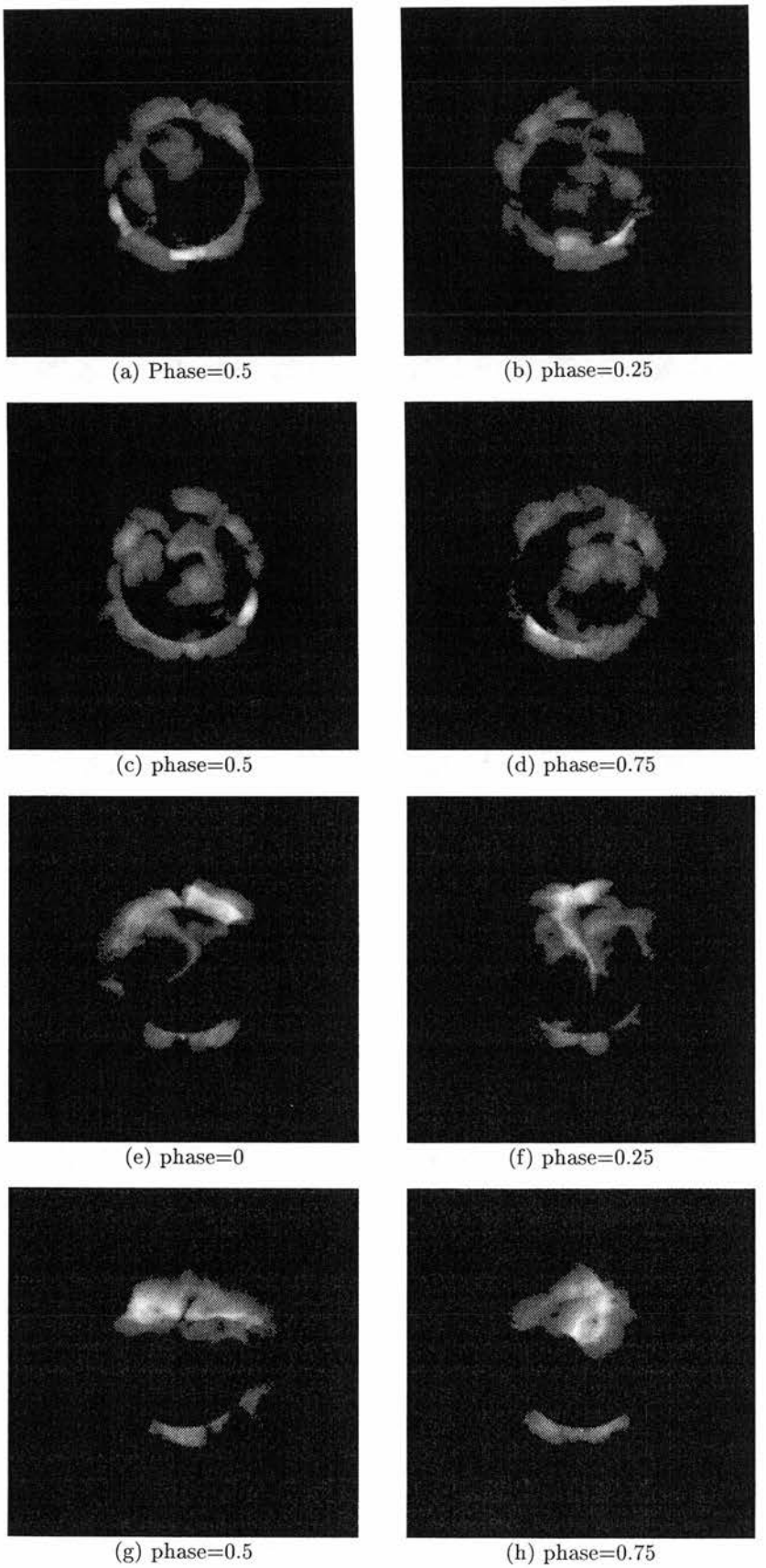

(a) Phase=0.5 (b) phase=0.25

(c) phase=0.5 (d) phase=0.75

(e) phase=0 (f) phase=0.25

(g) phase=0.5 (h) phase=0.75

Figure 5.4: The X-ray emission for the overlapping butterfly diagram (case (b) in Fig.1. (a)-(d) show the emission corresponding to a maximum in the rotational modulation while (e)-(h) correspond to a minimum. Emission measures are for coronal temperature of $10^7 K$. The inclination is set at 60°.

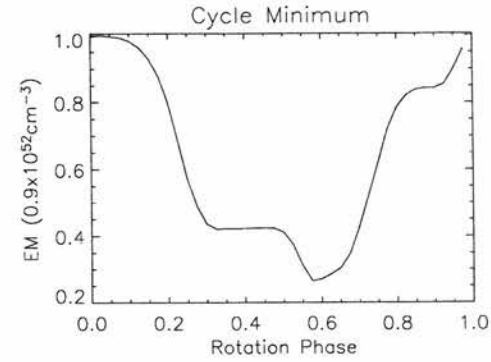

(a)

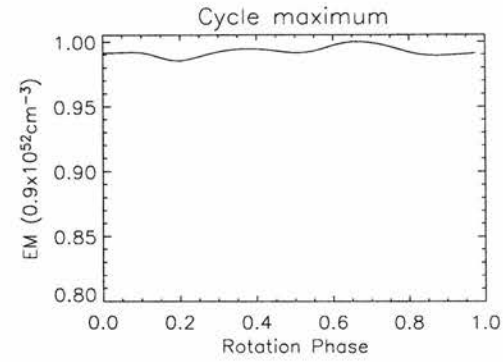

(b)

Figure 5.5: Examples of maximum and minimum values of the rotational modulation from the overlapping butterfly model. Figure (a) is taken from early in the 11 year cycle and corresponds to figures 3(a)-3(d). Figure (b) is about midway through the cycle and corresponds to Figures 3(e)-3(h).

from XMM-Newton observations (Güdel et al., 2001). Unlike the X-ray emission there is very little variation in the density. We can possibly see a variation of half an order of magnitude in the density for the butterfly and no butterfly models but if we are to assume that $EM \propto {n_e}^2$ then this does not explain the 2 orders of magitude variation seen the X-ray emssion. The reason for the increased emission is then due to the volume of the emitting region. During cycle maximum the increase in emerging bipoles allows for more closed coronal loops which lead to more regions of X-ray emission.

It can also be seen from Figs.5.2(d),5.2(c),5.2(b) that the rotational modulation is greater during the cycle minimum. This is represented by the grey shading in these Figures, illustrating the maximum and minimum values of emission throughout one rotation of the star for each point in the cycle. The rotaional modulation can be seen to vary considerably, although calculating an average over the cycle we find the overlapping butterfly to have the

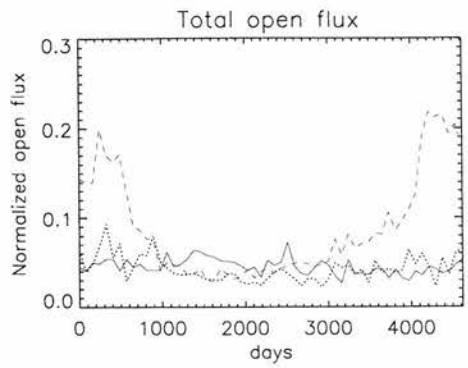

(a)

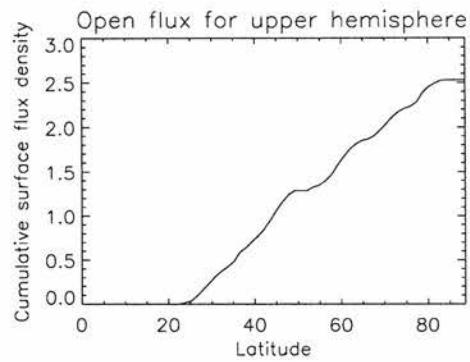

(b)

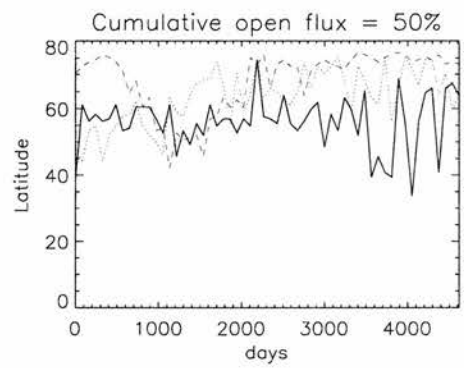

(c)

Figure 5.6: (a) shows the variation of the open magnetic flux over a cycle. The solid line represents the overlapping butterfly model, the dashed line represents the model where no butterfly diagram is used and the dotted line represents the model using the butterfly diagram. (b) is an example of the distribution of open flux for the overlapping butterlfy midway through the cycle. By cumulatively adding the openflux as we step up in latitude we can determine at which latitude the open flux is 50% of the total open flux. This gives a good indication as to where the majority of open flux lies with respect to latitude. The latitude where the cumulative open flux equals 50% is then plotted in (c) thus giving an indication of the movement of open flux over the whole cycle.

least with a value of only 21%. Observations estimate the rotational modulation for AB Dor to lie in the range of $5 - 15\%$ (Kuerster et al., 1997). Although this is less than that calculated in these models it is reassuring that the overlapping butterfly (i.e the model that best emulates observable features seen on AB Dor) produces the least rotational modulation of the three. There is a trend for all three models to show a decrease in the rotational modulation during the maximum of the cycle. Again, this is to be expected, as more surface flux at this point in the cycle with no increase in open flux means that there is an abundance of closed loops. For the rotational modulation to be low there must be a steady amount of these closed loops all round the star, so as the star rotates there is little fluctuation in the emission. To explain the large peaks and low troughs seen in the rotational modulation we have taken examples from the overlapping butterfly and constructed X-ray images as seen in Fig.5.4. The corresponding plots of the rotational modulation can be seen in Fig.5.5. It is easily seen that the high rotaional modulation is produced when flux and also X-ray emission is present at low latitudes. These regions of emission can be self eclipsed by the star and so produce larger values of rotational modulation. In cases of low rotational modulation the flux is seen to be concentrated at high latitudes. These regions remain in view as the star rotates due to the stellar inclination of $60°$ (the same inclination as AB Dor).

5.3.2 Open flux

In the case where no butterfly diagram was used a variation in the amount of open flux can also be seen, with an increase evident at the beginning and end of the cycle Fig.5.6(a). This increase is due to the bipoles becoming more sparse accross the stellar surface at these points of the cycle. As such field lines that were able to connect to nearby opposite polarities are now forced to traverse further across the star and hence stretch out to higher regions where the gas pressure overpowers the magnetic pressure and so forces the field lines to open. We do not see this increase in open field for the butterfly or overlapping butterfly because in both these cases, bipoles remain in a fairly close proximity to each other as determined by the width of the butterfly pattern. Fig.5.6(b) is an example of the distribution of open flux midway through the cycle for the overlapping butterfly model. For convenience we only look at the upper hemisphere of the star assuming a symmetry about the equator due to the nature of our models. Moving towards the pole of the star from the

equator we can see that there is no open flux at all until a latitude of 23°. The constant gradient up to 80° in the cumulative flux of Fig.5.6(b) shows that the distribution of open flux is fairly constant over this latitude range. There is no increase in the cumulative open flux above 80° due to strong intermingling of positive/negative flux in the polar fields at high latitudes. By taking the latitude where the cumulative open flux amounts to 50% of the total open flux, for each step in the cycle, we produce the plot seen in Fig.5.6(c). This shows how the distribution of open flux varies with latitude throughout the cycle. There seems to be no obvious pattern for cyclic behaviour in any of the models for the distribution of open flux. However the location of open flux with respect to latitude has important implications when considering the amount of angular momentum loss and mass loss from the star. Holzwarth et al. (2005) has shown that open field lines which are rooted nearer the equator will lead to greater angular momentum loss and mass loss from the star. The models here do show variation in the latitude of open flux accross the cycle but no real pattern of cyclic behaviour. However the open flux is at significantly lower latitudes for the overlapping butterfly than the other two models. This means that the angular momentum loss and mass loss from our model star's do not follow the cycle seen in the total flux and X-ray emission.

5.4 Conclusions

In this chapter we have used simulations of the surface magnetic field from the paper of (Mackay et al., 2004) along with the potential field approximation to consider the variation of X-ray emission and open flux for the type of cycles and flux emergence profiles that sucessfully reproduce the intermingling of opposite flux at high latitudes such as is observed on rapidly rotating solar like stars. From this we were able to determine how different types of cycles and emergence profiles affect the X-ray emission which in future could be used to test the models with observations.

We have shown how the open flux of our models varies over the magetic cycle as well as the distribution of openflux in latitude. In all three cases the distribution of open flux shows no cyclic behaviour. This suggests that any mass loss and angular momentum loss will equally show no cyclic variation. It is clear however that the case of the overlapping butterfly has open flux at significantly lower latitudes than the other models. This would

then lead to significantly more loss of angular momentum, by the model of Holzwarth et al. (2005).

We also find that for models where we used a butterfly and no butterfly pattern, X-ray emission shows a variation consistent with the magnetic cycle. In the case of an overlapping butterfly model there is no obvious cycle in the X-ray emission. The lack of cycles seen in observations of the X-ray emission in young rapidly rotating stars is emphasised in these models. However, a lack of cyclic behaviour in the X-ray emssion does not mean that there is no magnetic cycle. From the flux emergence simulations of Mackay et al. (2004) it was found that an overlapping butterfly model best produced the observable features such as high latitude intermingling of polarities. It is with this same model that we find no cyclic behaviour in the the total magnetic flux and the X-ray emission. This is in good agreement with the results from current programs looking for X-ray cycles which suggest a lack of X-ray variability in active stars. The rotational modulation however can be seen to vary over the cycle in all three models. It remains low through most of the cycle but rising relatively high when the stars are least active. Observations of the star AB Dor have shown low rotational modulation in the X-ray emission. If AB Dor does have a cycle then our models imply that observations to date may have been viewing AB Dor at a very active point in its cycle.The similar yet less active star EK Dra, however, shows much stronger rotational modulation in the X-ray emission (Guedel et al., 1995) and indications of a cycle (Berdyugina & Järvinen, 2005). These factors would be consistent with either a butterfly or no butterfly model. Longer term observations of more stars would be needed to determine if this apparent difference in magnetic cycles is a consequence of the decrease in rotation rate as stars age.

CHAPTER 6

Extrasolar planets, stellar winds and chromospheric hotspots

6.1 Introduction

Here we focus on the structure of the star's magnetic field and its possible interaction with an orbiting planet. This is in contrast to the approach of Ip et al. (2004), where the constructed model examined the nature of a planetary magnetic field caught in the stellar wind. For every point along the planet's orbit, we calculate the footpoints of those fieldlines that connect the star and planet. These are the locations where we would expect to see the chromospheric signature of reconnection between the magnetic fields of the star and the planet. This chapter aims to determine if such an interaction can reproduce the variation of the emission profile observed by Shkolnik et al. (2003). In addition we demonstrate the possible effects of different system geometries on the observable signature, and investigate possible origins for the observed phase lag between the emission peak and the planet's position.

6.2 Dipole fields for the stellar corona

The model for the stellar magnetic field is not strictly dipolar. In the case of a true dipole all field lines are closed. At some height however, the gas pressure will exceed the magnetic pressure and coronal plasma will escape to form the stellar wind (Mestel & Spruit, 1987). For a hydrostatic corona with typical solar parameters this happens at a height of $2.5R_\star$. As shown in Fig. 1 we allow for the opening up of field lines by introducing a source surface at some height R_s above the star, beyond which we assume the field is radial (Newkirk & Altschuler, 1969). Since HD 179949 is fairly solar like in its spectral type (F8V) and

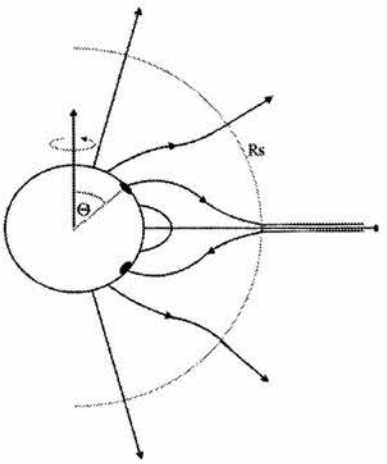

Figure 6.1: Magnetic structure of a dipole field where the magnetic axis is aligned with the stellar rotation axis. Beyond the source surface $R_s = 2.5R_\star$, the pressure of the hot coronal gas is large enough to force open the magnetic field lines. Shown are the surface spots that mark the footpoints of those field lines intercepted by a planet orbiting in the equatorial plane. If the coronal temperature and hence pressure is increased, or the stellar field strength is decreased, the source surface moves inwards and the angle Θ increases. The projected spot area is largest when the angle of inclination between the stellar rotation axis and the observer is equals the co-latitude Θ of the spot.

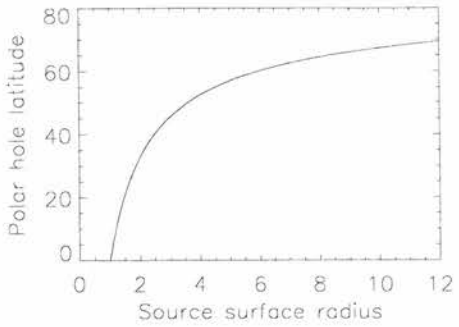

Figure 6.2: Change in latitude Θ of the edge of the polar hole as a function of source surface radius (R_s). Our model assumes that field lines originating from the stellar surface at this latitude will interact with the planet.

activity levels and rotates reasonably slowly ($P_{rot} = 9days$), we place the source surface at $r = 2.5R_\star$, which is the value used for similiar models of the Sun (Schrijver et al., 2003). Given that the orbit of the planet in HD 179949 is at $8.5R_\star$, this suggests that the planet moves through the open field of the star, not through the closed corona. We extrapolate the coronal field structure as outlined in chapter 2. In the case of a dipolar field we take the l=1, m=0 component of eqn.(2.13) and impose that at the stellar surface the field is dipolar, while at $r = R_s$ it is purely radial, i.e.

$$B_r(r = R_\star) = 2M \cos\theta / R^3, \tag{6.1}$$

$$B_\theta(r = R_s) = 0, \tag{6.2}$$

where M is the dipole moment defined as $M = B_r(r = R_\star, \theta = 0){R_\star}^3/2$. The field configuration is written in terms of a correction to the classical dipole field which allows for the effect of the source surface:

$$B_r = \frac{2M\cos\theta}{r^3} f(r, R_s), \qquad B_\theta = \frac{M\sin\theta}{r^3} g(r, R_s) \tag{6.3}$$

where

$$f(r, R_s) = \left(\frac{r^3 + 2{R_s}^3}{{R_\star}^3 + 2{R_s}^3} \right) \tag{6.4}$$

$$g(r, R_s) = \left(\frac{-2r^3 + 2{R_s}^3}{{R_\star}^3 + 2{R_s}^3} \right). \tag{6.5}$$

In the limit $R_s \to \infty$, we recover a dipolar field. The path of a field line is given by $\sin^2\theta = Ar/(r^3 + 2{R_s}^3)$. The last closed field line, that is the field line at the edge of the polar hole, passes through $\theta = \pi/2$ close to $r = R_s$ and so for this field line $A = 3{R_s}^2$. It

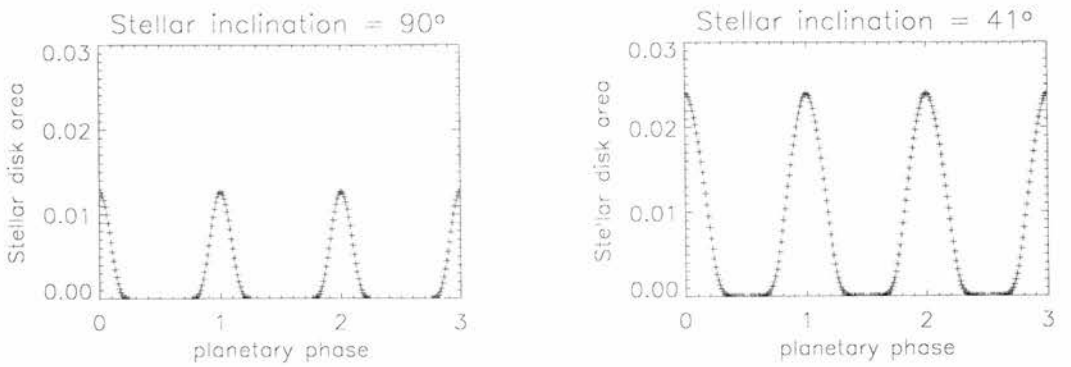

(a) (b)

Figure 6.3: Fractional projected area of spots as a function of planetary phase for a star with a dipole field. The rotation and orbital periods are 9 and 3 days respectively. The source surface in both cases here is at a distance of $2.5R_\star$. The cases (a) and (b) have an inclination of 90° and 41° respectively.

then follows that the last closed field line will connect to the stellar surface at a latitude which is dependent entirely on the location of the source surface (see Fig. 6.2).

6.3 Determining the location of surface emission features

The latitude Θ is then a lower limit to which open field lines can connect. We map the open field of the star by determining the longitude and latitude of the planet throughout its orbit and then tracing from these coordinates back to the stellar surface along the path of the magnetic field. Fig. 6.1 shows a star with an aligned dipole. We propose that open field lines interact with the planet's magnetic field and in turn produce an enhanced chromospheric emission at the footpoints. We assume that each planetary-stellar interaction releases the same amount of energy at the chromosphere. Following this assumption we also assume that the energy is radiated from an area at the chromosphere that is proportional to this energy. Neglecting the effect of limb darkening we then calculate the apparent size of the bright spot as seen on the stellar disk and take this as a proxy for the magnitude of the CaII emission. From the observer's point of view the magnitude of the emission will be greatest when the footpoint lies at disc centre and least if it lies at the stellar limb. Obviously no emission will be observed if the footpoint of the field line is hidden by the star and not on the visible stellar disc. We would also like to note that our model does not account for any time taken for the energy to disipate at the chromosphere.

Instead we have assumed that a bright patch will persist for as long as the planet and stellar field line are connected.

6.4 Results

6.4.1 An aligned dipole field

To get some bearings on this problem we will start with a star that has an aligned dipole and a source surface at $2.5R_\star$. We also adopt the observed orbital and rotation parameters for HD 179949 ($P_{orb} = 3$ days, $P_{rot} = 9$ days). We assume that the stellar rotation axis and orbital axis are aligned. Since the field is radial past the source surface, departures from a circular orbit would have no effect on the pattern of surface emission and so we neglect them. In our model we trace open field lines from the equatorial plane at the source surface. For an aligned dipole model this will give two possible latitudes for the footpoints on the stellar surface, at similiar latitudes in the northern and southern hemisphere, respectively. lower hemisphere. We assume a quasi-continous interaction between the open field lines from the star and the planet's magnetic field. Fig. 6.3(a) shows the normalized projected area of bright spots on the stellar surface, which we take as a proxy for the magnitude of the CaII flux. The peak of emission or projected area occurs when the planet is directly in front of the star (i.e. at inferior conjunction). The consistency in the magnitude of the emission through three of the planets orbits is attributed to the fact that the latitude of the footpoints remains constant from the observers perspective. A source surface of $2.5R_\star$ means that the minimum latitude for emission will be at $41°$ whereas a source surface at $10R_\star$ will have a minimum latitude of $67°$. The effect of the source surface on the latitude where the open field lines originate are shown in Fig. 6.2. This has a strong effect on the overall emission as the projected area becomes smaller with increasing distance of the source surface. The profile of the projected area however, consistently peaks at the sub-planetary point, independent from the postion of the source surface.

6.4.2 Tilting of the dipole and stellar inclination

For the case of a tilted dipole Eq.(6.3) becomes

$$B_r = 2M/r^3(cos\,\beta\,cos\,\theta + sin\,\beta\,cos\,\phi\,sin\,\beta)f(r, R_s) \tag{6.6}$$

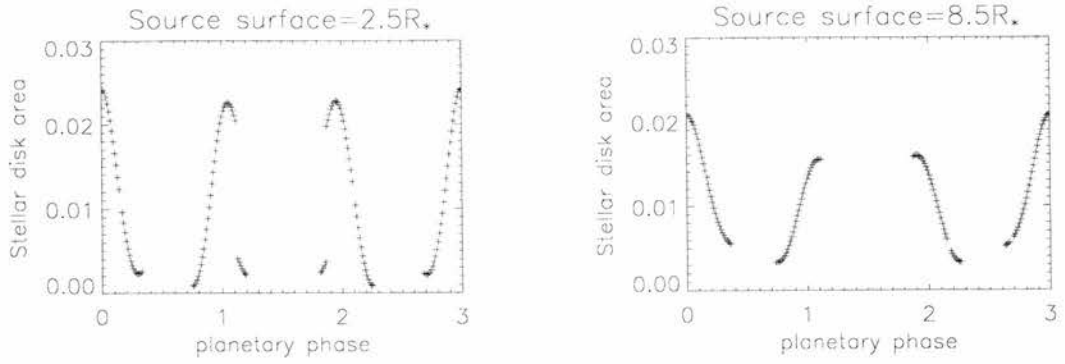

(a) (b)

Figure 6.4: Fractional projected area of spots as a function of planetary phase for a star with a dipole field tilted over at 45° to the rotation axis. Both (a) and (b) have an inclination of 83°. The peak in emission is out of phase with the planet for both cases. A greater phase shift is seen for (b) where the source surface is further out at $8.5R_\star$.The gaps seen in the figures are caused by the planet connecting with adjacent field lines that are rooted in opposite hemispheres.

where β is the angle between the dipole axis and the stellar rotation axis. The equation for a field line extending from the source surface in the equatorial plane is then

$$\cos\beta\cos\theta + \cos\phi\sin\beta\sin\theta = \sqrt{\frac{1-3\bar{R}_s^2(\cos\phi^2\sin\beta^2)}{1+2\bar{R}_s^3}}. \tag{6.7}$$

$\bar{R}_s = R_s/R_\star$ where $R_\star$ is the stellar radius and R_s is the source surface. Shkolnik et al. (2003) showed that the best fitting spot model requires the bright spot to be at 30° and a stellar inclination angle of 87°. However, observations show no transits for this system so an upper limit for the orbital inclination is set at 83° (Tinney et al., 2001). They also assumed that the orbital and stellar inclination angles would be comparable. Fig. 6.3(b) illustrates the effect of stellar inclination on the projected spot area. While the periodicity of the profile is not affected, as the inclination decreases from 90° the range of projected area increases, hitting a maximum at $i = 41°$ for $R_s = 2.5R_\star$.

By tilting the dipole axis relative to the rotation axis we can produce phase gaps in the peaks of the projected spot area. Figs. 6.4(a) and 6.4(b) show the projected spot area for a star with an inclination set to 83° and the dipole axis tilted over by 45° relative to the rotation axis. The phase gap for Fig. 6.4(a) is small at only 0.05 whereas pushing the source surface further out $8.5R_\star$ increases the phase gap to about 0.07. In both cases however the gap between the peak of the projected spot area and the phase of the planet

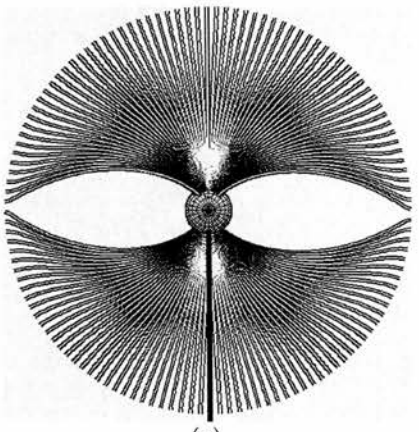

(a)

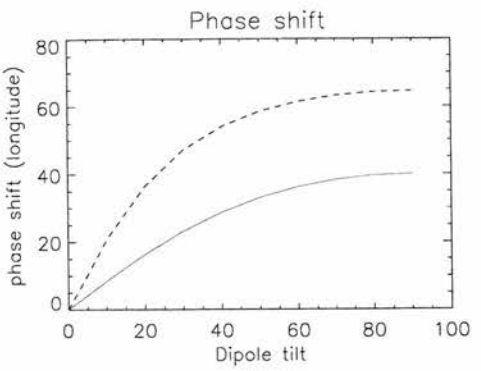

(b)

Figure 6.5: (a) dipole field tilted at 45° to the rotation axis. The view is looking down on the rotation axis. The thick black line represents the phase 0.0. (b) maximum phase shifts possible between the planetary phase and peak of the projected spot area as a function of dipole tilt. The solid represents a star with source surface at $2.5R_\star$ and the dashed line at $8.5R_\star$.

is not consistent. At planetary phase 0 and 3 there is no phase gap, while at phase 1 the peak in projected spot area lags behind the planet and at phase 2 preceeds the planet. The profiles produced by this model all repeat at 3 planetary phases, this is due to the fact that the orbital period of the planet is almost an exact multiple of the rotation period of star. From Shkolnik et al. (2003) the gap between observations of HD 179949 was 108 planetary orbits. This means that if there is a cycle over three planetary orbits, the observations of HD 179949 are at the same phase in this cycle (108/3 =36). Fig. 6.5(a) shows the curvature of the magnetic field lines due to the tilted dipole with a source surface at $8.5R_\star$. We can see from this that the longitude where we start the planet's orbits will affect the magnitude of the phase gaps seen at each planetary phase. This must be taken into account since this model assumes an ideal situation whereby the planets orbital period is an exact multiple of the stellar rotation period. Any deviation from this exactness in the periods will lead to variations of the phase gaps aswell as changes in the magnitude of the peaks. For this reason we have constructed the plot in Fig. 6.5(b). The maximum phase shift refers to a specific alignment. A surface spot being located at disk center from the observers perspective while the open field line extending from this spot has the maximum amount of curvature to the planets position. Fig. 6.5(b) shows clearly that by increasing the amount of tilt of the dipole the maximum possible phase gap also increases. It is also evident that moving the source surface further out, and hence allowing

more curvature of the field lines, we can also produce greater phase gaps. We should note that in the limiting case where $R_s \to \infty$ and the dipole is tilted at a maximum of 90° a maximum phase gap of 90° can be achieved.

6.4.3 Wind torques and phase lags

The observations of Shkolnik et al. (2004) show that in the case of HD179949 the planet lags behind the peak of emission by almost 60°, whereas in the case of υ And the planet lies almost at the another side of the star, lagging behind by 169°. The model presented in this chapter for a planet at $8.5R_\star$ the maximum possible phase lag between the chromospheric emission and planet is about 65°. While this maximum can go someway in explaining the phase lags seen at HD179949 it cannot explain the very large phase lags seen at υ And. In an attempt to further explain the observation of phase lags we apply a magnetic stellar wind model, in which open field lines extending out beyond the orbit of the planet, are bent in a retrograde direction forming spirals around the stellar rotation axis. We estimate this phase lag using solar values for the surface field strength and pressure along with the observed values for the stellar mass, radius and rotation rate. According to basic magnetised wind theory, the phase lag between the footpoint of a field line and its crossing point at the planet's orbit is given by

$$\Phi = \int_{x_\star}^{x_p} -\frac{r_a \Omega}{V_a} \frac{1-x^2}{1-x^2 u}\, dx. \tag{6.8}$$

Φ is the phase lag and $x = r/r_a$ and $u = V_r/V_a$. r_a is the Alfvenic point, V_r and V_a are the radial and Alfvenic velocities, respectively. Ω is the stellar rotation (Mestel, 1999).

For a reasonable range of values of magnetic field strength (2 to 200 Gauss), the maximum phase gap at a distance of $8.5R_\star$ is $\leq 6°$. To reach a phase lag of 60° the planet would need to be much further out, at approximately $100R_\star$. The phase gap is also increased if we include the travel time between the planet and star. If, as Shkolnik et al. (2004) discuss, a disturbance travels at the Alfvén speed, then it takes approximately a few hours to travel from the hot Jupiter to the stellar surface. In the model present here, however, we assume that the reconnection between the fields of the planet and the star accelerates electrons along the reconnected magnetic field lines. As in the case of a solar flare, these electrons impact on the stellar surface, causing the observed emission. Since the electron speed is so much greater than the Alfvén speed, however, the additional effect on the phase lag is negligible.

One possible improvement in the present model would be to replace the simple field structure used here with a physically-realistic field determined by extrapolating a surface magnetogram, as has been done for the Sun for many years and more recently for more active stars using Zeeman-Doppler images (Hussain et al., 2001). The use of a more complex field structure may not, however, help to reconcile the apparent phase lags reported at some epochs with the predictions of basic stellar wind theory. It is difficult to envisage any field structure that could support a large-scale, persistent azimuthal field at the orbits of these planets, strong enough to give consistent phase lags of 60 degrees or more.

6.5 Conclusions

Our model shows that a dipole field on a star with an inclination of about 83° can produce an emission variation with rotational phase whose form is consistent with observations of enhanced emission on the star HD179949 (Shkolnik et al., 2003). This model can also reproduce the phase shifts between the emission peak and the phase where the planet is directly in front of the star, reported by Shkolnik et al (2003). However, we are unable to reproduce the much larger phase shifts observed at υ And.

We investigate three factors that affect the variation of the emission.

- Cooling the corona or increasing the stellar field strength increases the extent of the closed corona and the latitude of the surface emission and hence reduces range of emission.
- Decreasing The stellar inclination increases the amplitude of the variation.
- A misalignment of the rotation and magnetic axis results in phase shifts up to 65° between the peak in emission and the sub-planetary point .

By varying these parameters it is possible to mimic the form of the reported flux variations (Shkolnik et al. 2003, 2004). For larger phase lags the model's source surface must stretch out to a height as big as the planets orbit along with extreme tilts to the dipole field. We have also determined the phase lag between the planet's location and the electron impact region on the star, using solar wind theory to model the spiral form imposed by torque

balance on the field-streamlines in the stellar wind. We find that lags of at most a few degrees in phase are possible for plausible estimates of the wind velocity, the Alfven radius and the stellar rotation rate.

CHAPTER 7

Summary and Future work

This work certainly provokes work for the future, in both theoretical studies and obervations. We have used observationally derived maps of the surface magnetic fields for the star's AB Dor and LQ Hya, provided by Zeeman-Doppler observations. In addition to this we have also looked simple dipole models which describe the surface field and more complex configurations obtained from flux emergence simulations. With these maps and assuming a potential field model, we have extrapolated the coronal field structure for the various models. Applying a gas law to the corona allows for the calculation of observable parameters such as the X-ray emission, rotaional modulation, coronal densities and, in the case of a star with an orbiting planet, locations of chromospheric emission.

In particuliar (chapter 3) we investigated the effect on the global field structure of AB Dor of adding field to the polar regions. We were able to conclude that the nature of the polar field does indeed make a difference to the global field structure. Current obeservations of the X-ray emission and prominence distribution however, are unable to discriminate between the different types of polar field. In chapter 4 we examined the similar young active star LQ Hya. We found that, unlike the sun, LQ Hya shows a significant change in the field structure from one year to the next. Despite this obvious change, values for its coronal density and X-ray emission remain relatively steady. Chapter 5 goes on to look at stellar cycles. The solar cycle is well documented but in stars other than the Sun observations of cycles are inconclusive. This chapter looked at 3 models of cyclic behaviour and the variation of X-ray emission and corresponding rotational modulation over each cycle. We find that our models agree with current observations of the star AB Dor where no cycle is observed.

In the forementioned chapters there is much room for refinement of the models and

a need for more observations. In the cases of AB Dor and LQ Hya we have shown that X-ray observations alone cannot provide a detailed account of the coronal structures. Advancements in the area of Zeeman-Doppler imaging along with observations from Doppler imaging, and photometric studies, could provide us with the level of detail needed to accurately discriminate between the variety of models proposed for these stars. There is also the possibility of Zeeman-Doppler imaging in the infrared. The cooler signature lines in this region of the spectrum could reveal some of the field of the ellusive dark polar caps.

Models presented in this thesis have assumed an isothermal corona, whereas in reality this is known not to be the case. Introducing a description of the temperature distribution in the corona will greatly aid the accuracy in calculating the X-ray emission of these star's. One possible model to describe the corona temperature would be to assign temperatures to loops based on their length or field strength or both. This may still be less than required however. X-ray images of coronal loop structures on the Sun reveal bright points at the base of coronal loops, which may require temperature stratification along each individual loop. The cyclic variations of chapter 5 could be looked at in more detail. In particular we have noticed in other chapters that the location of the source surface can have an impact on locations of open and closed field and hence X-ray emission and modulation. Future work could include a parameter study looking at how the source surface and coronal temperature affects the cyclic behaviour seen in the X-ray emission.

In chapter 6 we have looked at the simple geometry of a dipole stellar field in conjuction with an orbiting planet. This model was able to produce a profile that was consistent with observations of HD 179949. This chapter is very much an introduction to the theory for this area of study. As such, much of the approximations that were used to simplify this model can be extended in a number of different ways. For instance, using a potential field model based on magnetic maps of a real star such as the Sun could lead to the larger phase shifts required without the need for such extreme tilts of the magentic axis. This reasoning is based on the solar field having more azimuthal components present than a simple dipole. Also our model assumed a uniform spot size at the surface of the star. We could include the effect that the spot size will be proportional to the ratio of stellar and planet magnetic fields. The model could also allow for the hotspots at the surface to dissipate away at a time determined by laws of radiative transfer.

Bibliography

Alekseev I. Y., Kozlova O. V., 2003, Astrophysics, 46, 28

Basri G., Marcy G. W., 1994, ApJ, 431, 844

Berdyugina S. V., Järvinen S. P., 2005, Astronomische Nachrichten, 326, 283

Berdyugina S. V., Pelt J., Tuominen I., 2002, A&A, 394, 505

Bray R. J., Cram L. E., Durrant C. J., 1991, Plasma loops in the solar corona. Cambridge Astrophysics Series, Cambridge: Cambridge University Press, 1991

Brickhouse N. S., Raymond J. C., Smith B. W., 1995, ApJs, 97, 551

Collier Cameron A., 1995, MNRAS, 275, 534

Collier Cameron A., Robinson R. D., 1989a, MNRAS, 236, 57

—, 1989b, MNRAS, 238, 657

Collier-Cameron A., Unruh Y. C., 1994, MNRAS, 269, 814

Cuntz M., Saar S. H., Musielak Z. E., 2000, ApJL, 533, L151

Cuntz M., Shkolnik E., 2002, Astronomische Nachrichten, 323, 387

Cutispoto G., Messina S., Rodonò M., 2001, A&A, 367, 910

Donati J.-F., 1999, MNRAS, 302, 457

Donati J.-F., Cameron A. C., Semel M., Hussain G. A. J., Petit P., Carter B. D., Marsden S. C., Mengel M., López Ariste A., Jeffers S. V., Rees D. E., 2003, MNRAS, 345, 1145

Donati J.-F., Collier Cameron A., 1997, MNRAS, 291, 1

Dupree A. K., 1993, Bulletin of the American Astronomical Society, 25, 856

Eggen O. J., 1984, aj, 89, 1358

Favata F., Micela G., Baliunas S. L., Schmitt J. H. M. M., Güdel M., Harnden, F. R., Sciortino S., Stern R. A., 2004, A&A, 418, L13

Fekel F. C., Bopp B. W., Africano J. L., Goodrich B. D., Palmer L. H., Quingley R., Simon T., 1986, aj, 92, 1150

Güdel M., Audard M., Briggs K., Haberl F., Magee H., Maggio A., Mewe R., Pallavicini R., Pye J., 2001, A&A, 365, L336

Granzer T., Schüssler M., Caligari P., Strassmeier K. G., 2000, A&A, 355, 1087

Guedel M., Schmitt J. H. M. M., Benz A. O., Elias N. M., 1995, A&A, 301, 201

Hussain G. A. J., Jardine M., Collier Cameron A., 2001, MNRAS, 322, 681

Hussain G. A. J., van Ballegooijen A. A., Jardine M., Cameron A. C., 2002, ApJ, 575, 1078

Ip W., Kopp A., Hu J., 2004, ApJL, 602, L53

Järvinen S. P., Berdyugina S. V., Tuominen I., Cutispoto G., Bos M., 2005, A&A, 432, 657

Jardine M., Collier Cameron A., Donati J.-F., 2002a, MNRAS, 333, 339

Jardine M., Collier Cameron A., Donati J.-F., Pointer G. R., 2001, MNRAS, 324, 201

Jardine M., Wood K., Collier Cameron A., Donati J.-F., Mackay D. H., 2002b, MNRAS, 336, 1364

Jetsu L., 1993, A&A, 276, 345

Kellett B. J., Bingham R., Cairns R. A., Tsikoudi V., 2002, MNRAS, 329, 102

Kitchatinov L. L., Jardine M., Donati J.-F., 2000, MNRAS, 318, 1171

Kuerster M., Schmitt J. H. M. M., Cutispoto G., Dennerl K., 1997, A&A, 320, 831

Linker J. A., Lionello R., Mikić Z., Amari T., 2001, jgr, 106, 25165

Linsky J. L., Gagne M., 2001, Bulletin of the American Astronomical Society, 33, 846

Lockwood M., 2003, Journal of Geophysical Research (Space Physics), 7

Lockwood M., Stamper R., Wild M. N., 1999, nat, 399, 437

Luhman K. L., Stauffer J. R., Mamajek E. E., 2005, ApJL, 628, L69

Mackay D. H., Jardine M., Cameron A. C., Donati J.-F., Hussain G. A. J., 2004, MNRAS, 354, 737

Mackay D. H., Priest E. R., Lockwood M., 2002, solphys, 209, 287

Maggio A., Pallavicini R., Reale F., Tagliaferri G., 2000, A&A, 356, 627

Marcy G. W., Butler R. P., 1998, in ASP Conf. Ser. 154: Cool Stars, Stellar Systems, and the Sun, pp. 9–+

Martens P. C. H., SADE Team, 2004, American Astronomical Society Meeting Abstracts, 204,

Mayor M., Queloz D., 1995, nat, 378, 355

McIvor T., Jardine M., Cameron A. C., Wood K., Donati J.-F., 2003, Mon. Not. Royal Astron. Soc., 345, 601

Mestel L., 1999, Oxford University Press

Mestel L., Spruit H. C., 1987, MNRAS, 226, 57

Micela G., Marino A., 2003, A&A, 404, 637

Newkirk G., Altschuler M., 1969, baas, 1, 288

Orlando S., Peres G., Reale F., 2004, A&A, 424, 677

Parker E. N., 1955, ApJ, 122, 293

Pointer G. R., Jardine M., Collier Cameron A., Donati J.-F., 2002, MNRAS, 330, 160

Rubenstein E. P., Schaefer B. E., 2000, ApJ, 529, 1031

Sanz-Forcada J., Brickhouse N. S., Dupree A. K., 2003a, ApJs, 145, 147

Sanz-Forcada J., Maggio A., Micela G., 2003b, A&A, 408, 1087

Schrijver C. J., DeRosa M. L., Title A. M., 2003, ApJ, 590, 493

Schrijver C. J., Title A. M., 2001, ApJ, 551, 1099

Schuessler M., Solanki S. K., 1992, A&A, 264, L13

Shkolnik E., Walker G. A. H., Bohlender D. A., Gu P. ., Kürster M., 2004, ArXiv Astrophysics e-prints

Shkolnik E., Walker G. A. H., Bohlender D. A., Rucinski S., 2003, American Astronomical Society Meeting, 203,

Smith E. J., Marsden R. G., Balogh A., Gloeckler G., Geiss J., McComas D. J., McKibben R. B., MacDowall R. J., Lanzerotti L. J., Krupp N., Krueger H., Landgraf M., 2003, Science, 302, 1165

Solanki S. K., Motamen S., Keppens R., 1997, A&A, 325, 1039

Solanki S. K., Schüssler M., Fligge M., 2002, A&A, 383, 706

Stern R. A., Alexander D., Acton L. W., 2003, in The Future of Cool-Star Astrophysics: 12th Cambridge Workshop on Cool Stars, Stellar Systems, and the Sun (2001 July 30 - August 3), eds. A. Brown, G.M. Harper, and T.R. Ayres, (University of Colorado), 2003, p. 906-911., pp. 906–911

Strassmeier K. G., 1996, in IAU Symp. 176: Stellar Surface Structure, p. 289

Tinney C. G., Butler R. P., Marcy G. W., Jones H. R. A., Penny A. J., Vogt S. S., Apps K., Henry G. W., 2001, ApJ, 551, 507

Unruh Y. C., Collier Cameron A., Cutispoto G., 1995, MNRAS, 277, 1145

van Ballegooijen A. A., Cartledge N. P., Priest E. R., 1998, ApJ, 501, 866

Vilhu O., Tsuru T., Collier Cameron A., Budding E., Banks T., Slee B., Ehrenfreund P., Foing B. H., 1993, A&A, 278, 467

Wang Y.-M., Lean J., Sheeley N. R., 2000, grl, 27, 505

Wang Y.-M., Sheeley N. R., Lean J., 2002, ApJ, 580, 1188

Erratum

Thomas McIvor

06/04/2006

In the thesis titled Stellar Magnetic Field the following additions and changes have been made: Page 1 line 15 - Should read inhibit convection and conduction

Page 2 line 4 - Should read Above the photosphere lies the chromosphere, a region transparent in optical wavelengths about 2500 kilometers thick. Line 13 - Should read The magnetic field expands and so the plasma with it. The plasma remains trapped by the frozen-in field condition. Line 21 - Should read Skylab, SMM and LASCO

Page 3 line 23 - Add in the following: The model simulates the photospheric magnetic field on very active cool stars using flux injection and surface distribution based on strictly solar parameters. This includes an 11 year sunspot cycle and associated butterfly pattern. The magnitude of the cycle was the only free parameter investigated. Line 26 - The following is also added: Schrijver & Title (2001) concluded that polar spots are consistent with a dynamo like Sun for a sufficiently enhanced emergence frequency of active regions.

Page 4 line 4 - The following is added: The technique is based on the analysis of high-resolution spectropolarimetric data and allows for disentangling magnetic field distribution on the stellar surface due to different Doppler shifts of Zeeman-split local line profiles in the spectrum of a rotating star. In the absence of rotation, the net circular polarisation signal in spectral lines would be zero due to mutual cancellations of contributions of regions of opposite field polarity. Zeeman signatures in atomic lines due to starspots are expected to be extremely small, with typical relative amplitudes of 0.1%. Detecting them requires measurements of polarisation with noise level in Stokes as low as 10^{-4}, while the current instrumentation allows for the best relative noise level of 10^{-3}. Semel (1989) and Semel and Li (1996) proposed a multi-line approach for increasing

the signal-to-noise (S/N) ratio of the measured polarisation, which has resulted in first detection of the circular polarisation signal in a cool star (Donati et al., 1997). A combination of Stokes profiles using a multi-line technique called Least Squares Deconvolution (LSD) is based on the weak field approximation, i.e., one assumes that the magnetic splitting of spectral lines is smaller than their local Doppler broadening.

Page 5 line 8 - Should read: Kitchatinov presented a model for the the differential rotation and dynamo activity on LQ Hya. The model predicts the distributions of angular velocity, meridional flow and entropy within a convection zone provided that stellar structure parameters are given. These parameters include the stellar mass, luminosity, radius, fractional radius of the convection zone base, density and temperature. This model reproduced many of the features seen on LQ Hya, such as the yearly changes in the global field structure and demonstrated that both axisymmetric and non-axisymmetric modes may be present, with the axisymmetric mode being favoured.

Page 5 at the beginning of 1.3 the wavelength of the X-ray emission is in the 0.5-4 keV range.

Page 7 line 15 - The word rotation should be replaced by revolution. Line 20 - The word accelerate should be replaced by travel.

Page 9 line 5 - Should read: The behaviour of such plasmas is governed by the following equations. Each equation should be labeled independently such that (2.1) Mass conservation (2.2) Momentum Conservation (2.3) Energy conservation (2.4) Perfect gas law (2.5) Ampere's law (2.6) Faraday's law (2.7) Ohm's law

Line 9 should continue with the definition of terms to include $\mathbf{j}$ is the current density, E is the electric field, $\mathbf{g}$ is the gravitational acceleration, L is the energy

loss function and is the net effect of all sources and sinks of energy, k_B is the Boltzmann constant, m is the mean particle mass and σ represents the electric conductivity.

Page 10 line 12 should read a typical velocity can be taken as the sound speed which is $\approx 10^5 ms^{-1}$

Page 11 line 8 - The following sentence should be added: Fourier analysis is used to calculate the coeffecients. Reference Altschuler M. D., Newkirk G., Jr, 1969, Solar Phys., 9, 131 for the method of extrapolating the potential field using spherical harmonics with the an imposed source surface.

Page 12 line 22 should include; and 60 is the stellar inclination for stars AB Dor and LQ Hya

Page 13 line 14 should read ; As we move out to greater heights from the star the expansion of the plasma increases as the gas pressure rises. Eventually the tension in the magnetic field is overcome and is forced to reconnect allowing the plasma to escape along the open field lines.

At the bottom of the page the following information should be added; The radiative transfer code essentially considers packets of photons and their interaction with the surrounding medium. This is done by considering an emitted photon and following as it travels a distance to see what happens to it next. The photon can either be absorbed or scattered. The first thing to consider is how far the photon will travel. This length scale is closely related to the mean free path of the photon which is calculated from the coronal density. The probability that the photon will be absorbed or scattered is then determined by the albedo of the interacting particles which in turn depends on the number densities and cross sections of the particles. The scattering angles and interaction lengths have

associated probability distribution functions and samples of these quantities are then taken randomly. For the calculations used to determine the X-ray emission 1×10^8 photons are initially released into the corona. We then reiterate the above steps till all photons have either been scattered away from the corona or absorbed. Absorbed photons do not contribute to the emergent flux but do contribute to the mean intensities as it scatters throughout the atmosphere until it is absorbed.

Page 16 line 14 should read ; the Zeeman signal is either suppressed or not detectable.

Page 18 fig 3.2(a) is the field configuration with nothing at the pole, (b) has a global dipole field, (c) is concentric rings and (d) has a bipole at the each pole.

Page 27 line 6 the following to be added; The idea here is that field lines rooted nearer the equator have a greater lever arm in which to propel matter from the star.

Page 28 line 17 should read; We can obtain a lower limit on the source surface... Page 28 line 19 should read; the simplest solution of equation (2.13), which ...

Page 29 line 5 should read; A test height for the source surface was deliberately over-estimated at $6R_\star$.

Page 29 line 27 should read; spherical harmonic decomposition of equation (2.13)

Page 32 line 5 should not have the word surprisingly at the beginning of the sentence

Page 33 line 14 the following is added before the reference to Smith et al. 2003; so that the axis of the magnetic dipole lies at 90° to the rotation axis.

Page 34 Reference to figures is incorrect. Fig.3a and Fig.3b should be replaced with Fig.4.3a and Fig.4.3b respectively. Fig.2b should read Fig.4.2b Also reference to overall flux function (1) is incorrect and should read equation (2.13).

Page 35 Reference to figures is incorrect. Fig.5.4 should be replaced with Fig.4.5

Page 50 The following should be added to the end of the introduction; Similar work has been done in studies looking at the interaction between Jupiter and Io. Clarke et al. (2002) studied the magnetic footprints on Jupiter's upper atmosphere that appear as spots of ultraviolet emission. The spots remain fixed underneath Io as Jupiter rotates and are believed to be caused by the electromagnetic interaction between Jupiter's magnetic field and the plasma surrounding Io. While the lack of any phase lag in the Jupiter-Io system makes the problem simpler the similarity of signatures seen at HD 179949 suggest that the observed chromospheric hotspots are also related to an electromagnetic interaction between the planet and star. Reference to Clarke J. T., 2002, Nature, 415, 994-996 should be added to the Bibliography.

Page 55 line 21. should read phase lag instead of phase gap.

Page 56 Fig.1 below should be added to Fig.6.5

Page 57 line 1. The word curvature should be replaced with the words phase lag

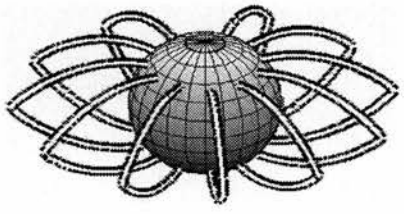

Figure 1: A simple dipole field where the magnetic axis and rotation axis are aligned. Inclination is set at 60° and the source surface is set at 2.5 stellar radii.